DUDLEY KNOX LIBRARY
NAVAL POSTGRADUATE SCHOOL
MONTEREY, CALIFORNIA 93943-5002

NAVAL POSTGRADUATE SCHOOL
Monterey, California

THESIS

AN ANALYSIS OF COHERENT AND DIFFERENTIALLY COHERENT DIGITAL RECEIVERS IN THE PRESENCE OF COLORED NOISE INTERFERENCE

by

Barry L. Shoop

September 1986

Thesis Advisor: Daniel Bukofzer

Approved for public release; distribution is unlimited

T232253

UNCLASSIFIED
ECURITY CLASSIFICATION OF THIS PAGE

REPORT DOCUMENTATION PAGE

a REPORT SECURITY CLASSIFICATION UNCLASSIFIED	1b. RESTRICTIVE MARKINGS
a SECURITY CLASSIFICATION AUTHORITY	3 DISTRIBUTION / AVAILABILITY OF REPORT Approved for public release; distribution is unlimited
b. DECLASSIFICATION / DOWNGRADING SCHEDULE	
PERFORMING ORGANIZATION REPORT NUMBER(S)	5. MONITORING ORGANIZATION REPORT NUMBER(S)
a. NAME OF PERFORMING ORGANIZATION aval Postgraduate School	6b OFFICE SYMBOL (If applicable) Code 62
7a. NAME OF MONITORING ORGANIZATION Naval Postgraduate School	
c. ADDRESS (City, State, and ZIP Code) onterey, California 93943-5000	7b. ADDRESS (City, State, and ZIP Code) Monterey, California 93943-5000
a NAME OF FUNDING / SPONSORING ORGANIZATION	8b. OFFICE SYMBOL (If applicable)
9 PROCUREMENT INSTRUMENT IDENTIFICATION NUMBER	
. ADDRESS (City, State, and ZIP Code)	10 SOURCE OF FUNDING NUMBERS

PROGRAM ELEMENT NO	PROJECT NO	TASK NO	WORK UNIT ACCESSION NO

TITLE (Include Security Classification)
N ANALYSIS OF COHERENT AND DIFFERENTIALLY COHERENT DIGITAL RECEIVERS
N THE PRESENCE OF COLORED NOISE INTERFERENCE

PERSONAL AUTHOR(S)
hoop, Barry L.

a TYPE OF REPORT	13b TIME COVERED	14 DATE OF REPORT (Year, Month, Day)	1S PAGE COUNT
ster's Thesis	FROM _____ TO _____	1986, September	115

SUPPLEMENTARY NOTATION

COSATI CODES		
FIELD	GROUP	SUB-GROUP

18 SUBJECT TERMS (Continue on reverse if necessary and identify by block number)
Optimum Colored Noise Jamming; MPSK; DPSK; MQAM

ABSTRACT (Continue on reverse if necessary and identify by block number)

Optimum receivers for detecting digital signals in additive white aussian noise are analyzed when operating in the presence of both white oise and colored noise interference. Modulation schemes, such as coherent -ary Phase Shift Keying (MPSK), Minimum Shift Keying (MSK), Differentially oherent Phase Shift Keying (DPSK), M-ary Quadrature Amplitude Modulation MQAM) and 16-state AM/PM are analyzed. Optimum power constrained colored oise interference spectra are developed for each modulation technique nalyzed so as to maximize the receiver error probability.

Receiver performance, quantified by bit and symbol error probabilities s numerically evaluated and graphically displayed as a function of signal-o-noise ratio and interference-to-signal ratio to demonstrate the effec-iveness of this interference in terms of the receiver performance egradation.

DISTRIBUTION / AVAILABILITY OF ABSTRACT	21 ABSTRACT SECURITY CLASSIFICATION
☒ UNCLASSIFIED/UNLIMITED ☐ SAME AS RPT. ☐ DTIC USERS	Unclassified

NAME OF RESPONSIBLE INDIVIDUAL	22b TELEPHONE (Include Area Code)	22c OFFICE SYMBOL
rof. Daniel Bukofzer	(408) 646-2859	Code 62Bh

FORM 1473, 84 MAR 83 APR edition may be used until exhausted
All other editions are obsolete

SECURITY CLASSIFICATION OF THIS PAGE
UNCLASSIFIED

Approved for public release; distribution is unlimited.

An Analysis of Coherent and Differentially Coherent Digital Receivers in the Presence of Colored Noise Interference

by

Barry L. Shoop
Captain, United States Army
B.S., The Pennsylvania State University, 1980

Submitted in partial fulfillment of the
requirements for the degree of

MASTER OF SCIENCE IN ELECTRICAL ENGINEERING

from the

NAVAL POSTGRADUATE SCHOOL
September 1986

ABSTRACT

Optimum receivers for detecting digital signals in additive white Guassian noise are analyzed when operating in the presence of both white noise and colored noise interference. Modulation schemes, such as coherent M-ary Phase Shift Keying (MPSK), Minimum Shift Keying (MSK), Differentially Coherent Phase Shift Keying (DPSK), M-ary Quadrature Amplitude Modulation (MQAM) and 16-state AM/PM are analyzed. Optimum power constrained colored noise interference spectra are developed for each modulation technique analyzed so as to maximize the receiver error probability.

Receiver performance, quantified by bit and symbol error probabilities is numerically evaluated and graphically displayed as a function of signal-to-noise ratio and interference-to-signal ratio to demonstrate the effectiveness of this interference in terms of the receiver performance degradation.

TABLE OF CONTENTS

LIST OF TABLES

LIST OF FIGURES

ACKNOWLEDGMENTS

I wish to express my sincere appreciation to my thesis advisor Professor Daniel Bukofzer for his guidance, patience and friendship during the research, composition, and completion of this thesis. This thesis is dedicated to my family; my wife, Linda, for her support and continual encouragement throughout my graduate education, and to my parents, Roy and Ruth Shoop, particularly my father whose wisdom, insight and counseling directed me into this field of study.

I. INTRODUCTION

Of the many different digital modulation methods that exist, each is designed and utilized so as to improve a particular feature of the communication system. Some such methods provide increased spectral efficiency while others improve overall system performance. Still others simplify the receiver structure and thereby reduce hardware costs. In order to prudently select the best modulation technique for a specific application, corresponding receivers must be analyzed and their performance compared using appropriate channel models. Although analyses of digital receiver performances abound in the literature, treatment is usually restricted to the case of additive white Gaussian noise (AWGN) as the channel interference. The AWGN model, although probably the easiest to analyze, seldom accurately describes an actual communication channel. For military applications, frequently a jamming environment must be assumed in which case the AWGN model is inadequate. While a great deal of effort has been devoted to the analysis and design of spread spectrum communication systems, virtually no documented receiver performance results exist for systems designed to operate in an AWGN interference that in practice must operate in the presence of a "smart" jammer.

In this thesis the performance of receivers operating in the presence of both AWGN and colored noise jamming is analyzed for several digital modulation techniques. Mathematical expressions for the receiver error rate performance are derived and optimized jamming techniques are developed for each receiver structure analyzed.

The receiver structures considered throughout are assumed to be optimally designed, in the sense of minimum probability of error performance in an AWGN environment. The colored noise jammer is modeled as Gaussian, power limited, uncorrelated with the white channel noise and with power spectral density determined as part of the optimization procedure.

Chapter II presents the derivation of symbol error probability for a coherent M-ary Phase Shift Keyed (MPSK) receiver operating in noise and jamming. Receiver performance curves are then presented for several values of M with jamming-to-signal ratio (JSR) as an independent variable to show the effectiveness of the optimized jammer. The optimum colored noise jammer applicable to this problem is developed in detail in this chapter.

In Chapter III the analysis carried out in Chapter II is applied to three very important special cases of MPSK signaling, namely Quadrature Phase Shift Keying (QPSK), Offset Quadrature Phase Shift Keying (OQPSK) and Minimum Shift Keying (MSK). The analysis presented here serves only to highlight

the differences between the MPSK techniques and the specific special case being considered.

The analysis in Chapter IV changes focus from coherent Phase Shift Keying to Differentially Coherent Phase Shift Keying (DPSK). In contrast to the purely mathematical development conducted in Chapter II, a geometric approach is used in order to simplify the analysis. Also, only the binary signaling case is considered. As in previous chapters, the mathematical expression for receiver performance is derived, error rate performance curves are presented and an optimized colored noise jammer is developed.

In Chapter V M-ary Quadrature Amplitude Modulation (MQAM) techniques are analyzed in the presence of colored noise jamming. Symbol error probability expressions are derived for the standard values of M = 16, 64 and 256 as well as for less typical M = 32. Receiver performance curves and optimized jamming waveforms are also included for each case so as to complete the analysis.

Chapter VI is devoted to the analysis of a digital radio transmission technique not treated in classical communication theory literature, namely a 16-state AM/PM signaling technique recommended by The International Telegraph and Telephone Consultative Committee (CCITT). Receiver performance is analyzed in the presence of AWGN both with and without colored noise jamming. The analysis of this signaling technique differs from those previously considered in that a suboptimum receiver

structure is assumed. The suboptimum receiver was chosen based on intuitive as well as practical considerations involving the implementation of the receiver logic. Also, due to the mathematically involved expressions for the symbol error probability, no jammer optimization is attempted. Comparisons between this 16 level signaling scheme and other (better known) 16 level schemes are presented.

Finally, Chapter VII provides performance comparisons and conclusions to be drawn from the analysis and graphical results obtained for the modulation methods considered in this thesis.

II. COHERENT M-ARY PHASE SHIFT KEYING

Coherent M-ary Phase Shift Keying (MPSK) is a digital signaling technique that provides bandwidth efficiency, constant signal envelope, relatively good error rate performance and simple receiver structures [Ref. 1]. MPSK is a signaling scheme that achieves its bandwidth efficiency at the expense of signal power.

A. SIGNAL DETECTION IN THE PRESENCE OF COLORED NOISE JAMMING

In MPSK modulation, the source transmits one of M signals, $s_i(t)$, $i = 1,2,\ldots,M$ every T_s seconds. The transmitted signal is of the form

$$s_i(t) = \sqrt{2E_s/T_s}\cos\left[2\pi f_0 t + \frac{2\pi(i-1)}{M} + \alpha\right] \qquad (2.1)$$

$$0 \leq t \leq T_s; \quad i = 1,2,\ldots,M$$

where E_s is the average signal set energy, α is an arbitrary, yet fixed phase and the information is contained in the $2\pi(i-1)/M$ phase term.

The optimum receiver for recovering the MPSK signal in the presence of AWGN is the maximum a posteriori (MAP) correlator receiver shown in Figure 2.1. This receiver is optimum in the sense of minimum probability of error.

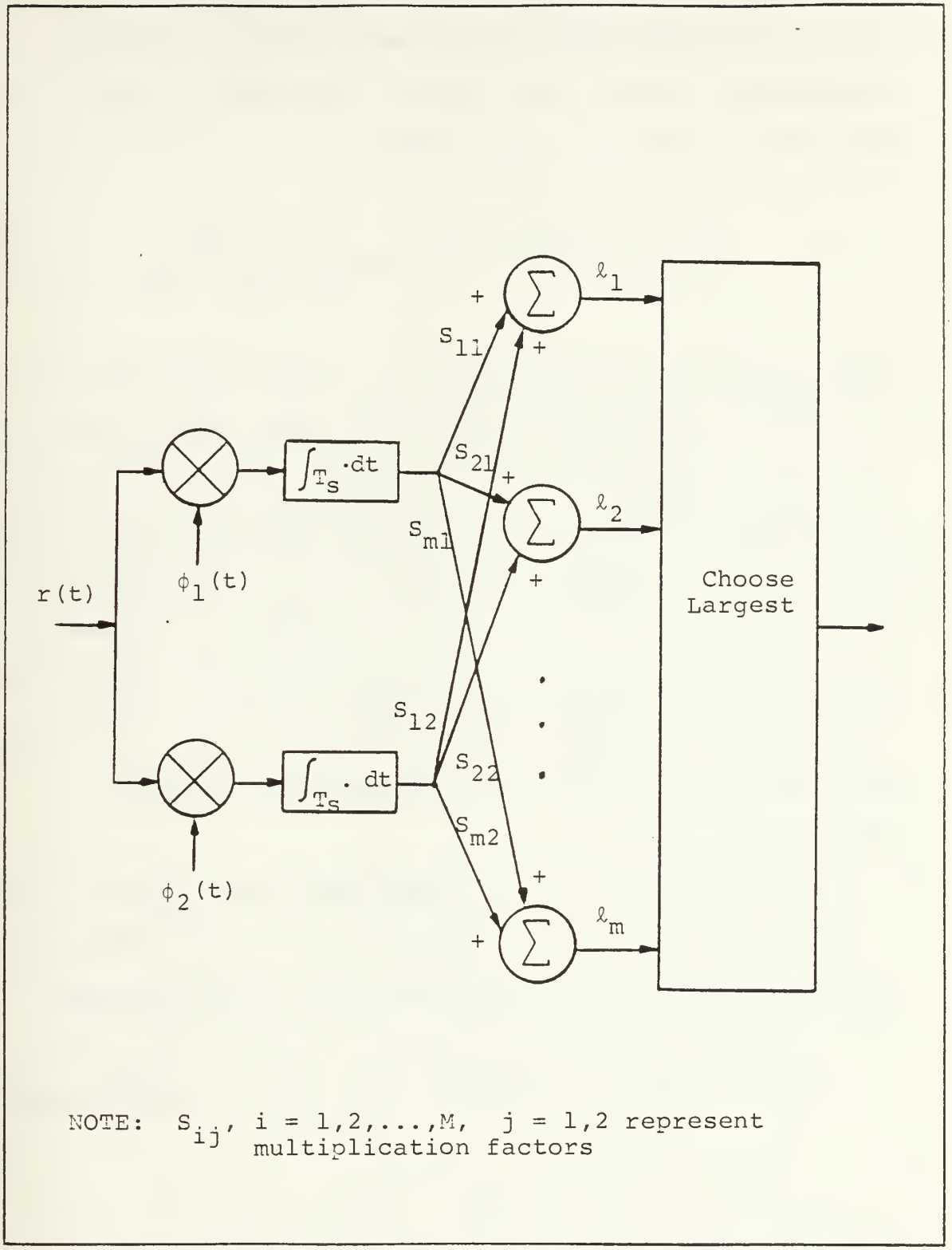

NOTE: S_{ij}, i = 1,2,...,M, j = 1,2 represent multiplication factors

Figure 2.1 Optimum MPSK Receiver for AWGN Channel

Because the signal is transmitted over a channel assumed to be corrupted by both white Gaussian noise and statistically independent colored noise jamming, the input to the receiver front end is the signal r(t), where

$$r(t) = s_i(t) + n_w(t) + n_c(t) \qquad 0 \leq t \leq T_s; \quad i = 1,2,\ldots,M \tag{2.2}$$

Here, $n_w(t)$ is a sample function of a white Gaussian noise process with zero mean and two-sided power spectral density level $N_0/2$ watts/Hz, and $n_c(t)$ is a sample function of a colored Gaussian noise process having autocorrelation function $K_c(\tau)$. Since the colored Gaussian noise is generated by a jammer operating independently of the AWGN in the channel, it is reasonable to assume that $n_c(t)$ and $n_w(t)$ are uncorrelated random processes. Because $n_c(t)$ and $n_w(t)$ have Gaussian amplitude statistics, the processes are statistically independent.

The receiver takes advantage of the fact that the transmitted signal $s_i(t)$ can be expressed as a linear combination of two orthonormal basis functions $\phi_1(t)$ and $\phi_2(t)$ where

$$\phi_1(t) = \sqrt{2/T_s}\cos(2\pi f_0 t+\alpha) \quad \text{and} \quad \phi_2(t) = \sqrt{2/T_s}\sin(2\pi f_0 t+\alpha) \tag{2.3}$$

Therefore,

$$s_i(t) = \sum_{n=1}^{2} S_{in}\phi_n(t) \qquad i = 1,2,\ldots,M \tag{2.4}$$

where

$$S_{in} = \int_0^{T_s} s_i(t)\phi_n(t)dt \qquad n = 1,2; \quad i = 1,2,\ldots,M \tag{2.5}$$

In the MPSK case being considered, the two basis functions were found by inspection. In more complicated modulation schemes it may be necessary to use techniques such as the Gramm-Schmitt orthonormalization procedure in order to determine the basis functions that allow a signal expansion of the form given by equation (2.4).

From $s_i(t)$ and the above definition, it is easily shown that

$$S_{i1} = \cos\frac{2\pi(i-1)}{M} \qquad i = 1,2,\ldots,M \tag{2.6}$$

$$S_{i2} = -\sin\frac{2\pi(i-1)}{M} \qquad i = 1,2,\ldots,M \tag{2.7}$$

Assuming equal prior probabilities for the transmitted signals, the receiver of Figure 2.1 computes and bases its decisions on

$$\ell_i = S_{i1}Y_1 + S_{i2}Y_2 \tag{2.8}$$

where

$$Y_j = \int_0^{T_s} r(t)\phi_j(t)dt \qquad j = 1,2 \tag{2.9}$$

Defining now

$$\theta_i \triangleq \frac{2\pi(i-1)}{M} \tag{2.10}$$

then

$$\ell_i = Y_1 \cos\theta_i - Y_2 \sin\theta_i = V\cos(\theta_i+\eta) \tag{2.11}$$

$$i = 1,2,\ldots,M$$

where

$$V = \sqrt{Y_1^2 + Y_2^2}\ ; \qquad \eta = \tan^{-1}(Y_2/Y_1) \tag{2.12}$$

A determination of the performance of the receiver of Figure 2.1 in terms of the probability of decision errors is now made by first observing that Y_1 and Y_2 are conditionally Gaussian random variables. Thus the mean of Y_1 and Y_2 conditioned on the signal $s_i(t)$ being sent is

$$E\{Y_1|s_i(t)\} = \sqrt{E_s}\, S_{i1} \tag{2.13}$$

$$E\{Y_2|s_i(t)\} = \sqrt{E_s}\, S_{i2} \tag{2.14}$$

and similarly, the conditional variance of Y_1 and Y_2 is

$$\sigma^2_{Y_1} = \frac{N_0}{2} + \int_0^{T_s}\int_0^{T_s} K_c(t-\tau)\phi_1(t)\phi_1(\tau)dt\, d\tau \tag{2.15}$$

$$\sigma^2_{Y_2} = \frac{N_0}{2} + \int_0^{T_s}\int_0^{T_s} K_c(t-\tau)\phi_2(t)\phi_2(\tau)dt\, d\tau \tag{2.16}$$

In Appendix A we demonstrate that

$$\int_0^{T_s}\int_0^{T_s} K_c(t-\tau)\phi_1(t)\phi_1(\tau)dtd\tau = \int_0^{T_s}\int_0^{T_s} K_c(t-\tau)\phi_2(t)\phi_2(\tau)dt\, d\tau \triangleq \sigma_c^2 \tag{2.17}$$

so that the conditional variance of Y_1 and Y_2 are identical.

Another important parameter which is an indication of how Y_1 and Y_2 are statistically related is the conditional cross covariance of Y_1 and Y_2, namely

$$E\{[Y_1-E\{Y_1\}][Y_2-E\{Y_2\}]\} = E\{n_{w_1} n_{w_2}\} + E\{n_{c_1} n_{c_2}\} \tag{2.18}$$

where

$$n_{w_j} = \int_0^{T_s} n_w(t)\phi_j(t)dt \; ; \quad n_{c_j} = \int_0^{T_s} n_c(t)\phi_j(t)dt \tag{2.19}$$

$$j = 1,2$$

It is simple to demonstrate that

$$E\{n_{w_1} n_{w_2}\} = 0 \tag{2.20}$$

while the second term in equation (2.18) which takes on the form

$$E\{n_{c_1} n_{c_2}\} = \int_0^{T_s} \int_0^{T_s} K_c(t-\tau)\phi_1(t)\phi_2(\tau)dt\, d\tau \tag{2.21}$$

needs more detailed analysis. First, we let

$$\phi_i'(t) = \begin{cases} \phi_i(t) & 0 \leq t \leq T_s \\ 0 & \text{otherwise} \end{cases} \tag{2.22}$$

so that $\phi_i'(t)$ is defined for all time t. Let $\Phi_i'(f)$ and $S_c(f)$ be the Fourier transforms of $\phi_i'(t)$ and $K_c(t)$, respectively. Thus we can show that

$$\int_0^{T_s} \int_0^{T_s} K_c(t-\tau)\phi_1(t)\phi_2(\tau)dtd\tau = \int_{-\infty}^{\infty} S_c(f)\Phi_1'(-f)\Phi_2'(f)df \tag{2.23}$$

From equation (2.3) it is clear that

$$|\Phi_1'(f)| = |\Phi_2'(f)| \tag{2.24}$$

and

$$\sigma_c^2 = \int_{-\infty}^{\infty} S_c(f) |\Phi_1'(f)|^2 df \tag{2.25}$$

This result will prove useful in obtaining the optimum jamming spectrum, $S_c(f)$.

We demonstrate in Appendix A that

$$E\{n_{c_1} n_{c_2}\} = 0 \tag{2.26}$$

so that

$$E\{[Y_1 - E\{Y_1\}][Y_2 - E\{Y_2\}]\} = 0 \tag{2.27}$$

which proves that Y_1 and Y_2 are uncorrelated. Since both Y_1 and Y_2 are conditionally Gaussian random variables, they are therefore statistically independent.

This fact makes the joint probability density function of Y_1 and Y_2 mathematically tractable. Using the general form for the probability density function (p.d.f.) of an N-dimensional Gaussian vector $\underline{x}$, namely

$$f_{\underline{x}}(\underline{x}) = \frac{1}{(2\pi)^{N/2} |\underset{\sim}{\Lambda}|^{1/2}} \exp\{-\frac{1}{2}(\underline{x}-\underline{m}_x)^T \underset{\sim}{\Lambda}_x^{-1} (\underline{x}-\underline{m}_x)\} \tag{2.28}$$

where

$$\underset{\sim}{m}_x = E\{\underline{x}\} \tag{2.29}$$

and

$$\underset{\sim}{\Lambda}_x = E\{(\underline{x}-\underline{m}_x)(\underline{x}-\underline{m}_x)^T\} \tag{2.30}$$

the joint p.d.f. of Y_1 and Y_2 can now be specified.

The case of MPSK under consideration is a two-dimensional problem where

$$\underline{m}_x = \begin{bmatrix} \sqrt{E_s}\, S_{i1} \\ \sqrt{E_s}\, S_{i2} \end{bmatrix} \qquad i = 1,2,\ldots,M \tag{2.31}$$

and

$$\underset{\sim}{\Lambda}_x = \begin{bmatrix} \sigma^2 & 0 \\ 0 & \sigma^2 \end{bmatrix} \quad ; \quad \sigma^2 = \frac{N_0}{2} + \sigma_c^2 \tag{2.32}$$

so that

$$|\underset{\sim}{\Lambda}_x| = [\frac{N_0}{2} + \sigma_c^2]^2 = \sigma^4 \tag{2.33}$$

From equation (2.32),

$$\underset{\sim}{\Lambda}_x^{-1} = \frac{1}{\sigma^2}\,\underset{\sim}{I} \tag{2.34}$$

where $\underset{\sim}{I}$ is a correspondingly dimensioned identity matrix. Thus, the conditional p.d.f. of Y_1 and Y_2, given that $s_i(t)$ was transmitted, becomes

$$f_{Y_1,Y_2|s_i(t)}(Y_1,Y_2|s_i(t)) = \frac{1}{2\pi\sigma^2}\exp\left\{-\frac{1}{2}\begin{bmatrix} Y_1-\sqrt{E_s}S_{i1} \\ Y_2-\sqrt{E_s}S_{i2}\end{bmatrix}^T \times \begin{bmatrix} 1/\sigma^2 & 0 \\ 0 & 1/\sigma^2\end{bmatrix}\begin{bmatrix} Y_1-\sqrt{E_s}S_{i1} \\ Y_2-\sqrt{E_s}S_{i2}\end{bmatrix}\right\} \qquad (2.35)$$

$$i = 1,2,\ldots,M$$

A double random variable transformation is now introduced, that is,

$$V = \sqrt{Y_1^2 + Y_2^2}\ ; \quad \eta = \tan^{-1}(Y_2/Y_1) \qquad (2.36)$$

This transformation leads to a new conditional p.d.f., namely

$$f_{V,H|s_i(t)}(v,\eta|s_i(t)) = vf_{Y_1,Y_2|s_i(t)}(v\cos\eta, v\sin\eta|s_i(t)) + vf_{Y_1,Y_2|s_i(t)}(-v\cos\eta,-v\sin\eta|s_i(t)) \qquad (2.37)$$

$$v \geq 0, \quad 0 \leq \eta \leq \pi$$

where from equation (2.35) we obtain

$$f_{V,H|s_i(t)}(v,\eta|s_i(t)) = \frac{v}{2\pi\sigma^2}\exp\left\{-\frac{1}{2}\begin{bmatrix} v\cos\eta-\sqrt{E_s}S_{i1} \\ v\sin\eta-\sqrt{E_s}S_{i2}\end{bmatrix}^T\right.$$

$$\left.\times\begin{bmatrix}1/\sigma^2 & 0\\ 0 & 1/\sigma^2\end{bmatrix}\begin{bmatrix} v\cos\eta-\sqrt{E_s}S_{i1} \\ v\sin\eta-\sqrt{E_s}S_{i2}\end{bmatrix}\right\}$$

$$+\frac{v}{2\pi\sigma^2}\exp\left\{-\frac{1}{2}\begin{bmatrix} -v\cos\eta-\sqrt{E_s}S_{i1} \\ -v\sin\eta-\sqrt{E_s}S_{i2}\end{bmatrix}^T\right.$$

$$\left.\times\begin{bmatrix}1/\sigma^2 & 0\\ 0 & 1/\sigma^2\end{bmatrix}\begin{bmatrix} -v\cos\eta-\sqrt{E_s}S_{i1} \\ -v\sin\eta-\sqrt{E_s}S_{i2}\end{bmatrix}\right\} \qquad (2.38)$$

$$v \geq 0, \quad 0 \leq \eta \leq \pi, \quad i = 1,2,\ldots,M$$

This p.d.f. can be simplified to the form

$$f_{V,H|s_i(t)}(v,\eta|s_i(t)) = \frac{v}{2\pi\sigma^2}\exp\{-\frac{1}{2\sigma^2}[v^2-2v\sqrt{E_s}\cos(\theta_j+\eta)+E_s]\}$$

$$+\frac{v}{2\pi\sigma^2}\exp\{-\frac{1}{2\sigma^2}[v^2-2v\sqrt{E_s}\cos(\theta_j+\eta+\pi)+E_s]\} \qquad (2.39)$$

$$v \geq 0, \quad 0 \leq \eta \leq \pi$$

It is apparent from the range of η that the two exponential terms in equation (2.39) can be replaced by a single exponential term by allowing η to range from 0 to 2π. Therefore we have finally,

$$f_{V,H|s_i(t)}(v,\eta|s_i(t)) = \frac{v}{2\pi\sigma^2}\exp\{-\frac{1}{2\sigma^2}[v^2-2v\sqrt{E_s}\cos(\theta_j+\eta)+E_s]\} \qquad (2.40)$$

$$v \geq 0, \quad 0 \leq \eta \leq 2\pi$$

The probability density function of η conditioned on $s_i(t)$ can be obtained by integrating equation (2.40) over the range of V, namely,

$$f_{H|s_i(t)}(\eta|s_i(t)) = \int_0^\infty \frac{v}{2\pi\sigma^2}\exp\{-\frac{1}{2\sigma^2}[v^2-2v\sqrt{E_s}\cos(\theta_j+\eta)+E_s]\}dv \qquad (2.41)$$

This integration results in

$$f_{H|s_i(t)}(\eta|s_i(t)) = \frac{1}{2\pi}\exp\{-\frac{E_s}{2\sigma^2}\sin^2(\theta_j+\eta)\}[\exp\{-\frac{E_s}{2\sigma^2}\cos^2(\theta_j+\eta)\}$$

$$+ \sqrt{2\pi E_s/\sigma^2}\cos(\theta_j+\eta)\,\mathrm{erf}_*\{\sqrt{E_s/\sigma^2}\cos(\theta_j+\eta)\}] \qquad (2.42)$$

where

$$\mathrm{erf}_*\{a\} = \int_{-\infty}^{a}\frac{1}{\sqrt{2\pi}}\exp\{-x^2/2\}dx = 1 - \mathrm{erfc}_*\{a\} \qquad (2.43)$$

Recalling from equation (2.11) that the decision rule was based on evaluating

$$\ell_i = V\cos(\theta_i+\eta) \qquad i = 1,2,\ldots,M \qquad (2.44)$$

and determining which of them is largest. Therefore, if $s_i(t)$ was sent, a correct decision will be made by the detector if

$$V\cos(\theta_i+\eta) > V\cos(\theta_j+\eta) \quad j = 1,2,\ldots,M; \quad i \neq j \tag{2.45}$$

Since $\cos(x)$ is a maximum when $|x|$ is a minimum, the decision rule can be modified to become

$$|\theta_i+\eta| < |\theta_j+\eta| \rightarrow \text{decide } s_i(t) \text{ was transmitted} \tag{2.46}$$

From equation (2.10) we have

$$\theta_i = \frac{2\pi(i-1)}{M} \qquad i = 1,2,\ldots,M \tag{2.47}$$

so that the condition of equation (2.46) is satisfied if

$$-\theta_i - \frac{\pi}{M} < \eta < -\theta_i + \frac{\pi}{M} \tag{2.48}$$

Therefore the probability of making a correct decision given that $s_i(t)$ was sent is

$$\Pr\{c|s_i(t)\} = \int_{-\theta_i-\pi/M}^{-\theta_i+\pi/M} f_{H|s_i(t)}(\psi|s_i(t))d\psi$$

$$= \int_{-\pi/M}^{\pi/M} f_{H|s_i(t)}(\beta-\theta_i|s_i(t))d\beta \tag{2.49}$$

From equation (2.42) we obtain

$$\Pr\{c|s_i(t)\} = \int_{-\pi/M}^{\pi/M} \frac{1}{2\pi}\exp\{-\frac{E_s}{2\sigma^2}\sin^2\beta\}\,[\exp\{-\frac{E_s}{2\sigma^2}\cos^2\beta\}$$

$$+ \sqrt{2\pi E_s/\sigma^2}\cos\beta\,\mathrm{erf}_*\{\sqrt{E_s/\sigma^2}\cos\beta\}]\,d\beta \qquad (2.50)$$

and defining

$$R_D \triangleq 2E_s/N_o: \quad \text{Signal power to Noise power Ratio (SNR)} \qquad (2.51)$$

$$R_J \triangleq \sigma_c^2/E_s: \quad \text{Jamming power to Signal power Ratio (JSR)} \qquad (2.52)$$

Since each signal was assumed to be equally likely, the desired result is

$$\Pr\{c\} = \frac{1}{M}\exp\{\frac{-R_D}{2(1+R_DR_J)}\} + \int_{-\pi/M}^{\pi/M} \sqrt{R_D/2\pi(1+R_DR_J)}\cos\beta$$

$$\times \exp\left\{\frac{-R_D\sin^2\beta}{2(1+R_DR_J)}\right\}\mathrm{erf}_*\{\sqrt{R_D/1+R_DR_J}\cos\beta\}\,d\beta \qquad (2.53)$$

This result specifies the performance of an MPSK receiver operating in an environment corrupted by both AWGN and colored noise jamming.

The probability of a symbol error is defined as

$$\Pr\{\varepsilon\} = 1 - \Pr\{c\} \qquad (2.54)$$

Observe that if the colored noise is not present, $R_J \equiv 0$, $\sigma^2 = N_0/2$, and equation (2.53) becomes the classical expression for the performance of an MPSK receiver in the presence of AWGN [Ref. 2], that is

$$Pr\{c\} = \frac{1}{M}\exp\{-\frac{E_s}{N_0}\} + \int_{-\pi/M}^{\pi/M} \sqrt{E_s/\pi N_0}\cos\beta\exp\{-\frac{E_s}{N_0}\sin^2\beta\}$$

$$\times \operatorname{erf}_*\{\sqrt{2E_s/N_0}\cos\beta\}d\beta \qquad (2.55)$$

Furthermore, if the jamming power were assumed to become infinitely large,

$$\lim_{R_J\to\infty} Pr\{c\} = \frac{1}{M} \qquad (2.56)$$

which, as expected, is the minimum value one can expect for a set of M equiprobable signals.

The results of equation (2.54) were numerically evaluated and plotted for the cases M = 4, 8, 16 and 32 in Figures 2.2 through 2.5, respectively. In each graph, the special case of JSR $\equiv$ 0.0 is included as a convenient reference to the performance of the particular received in AWGN interference only.

Now that an expression for the performance of an MPSK receiver in the presence of colored noise jamming has been derived, we next optimize the jammer in such a way as to

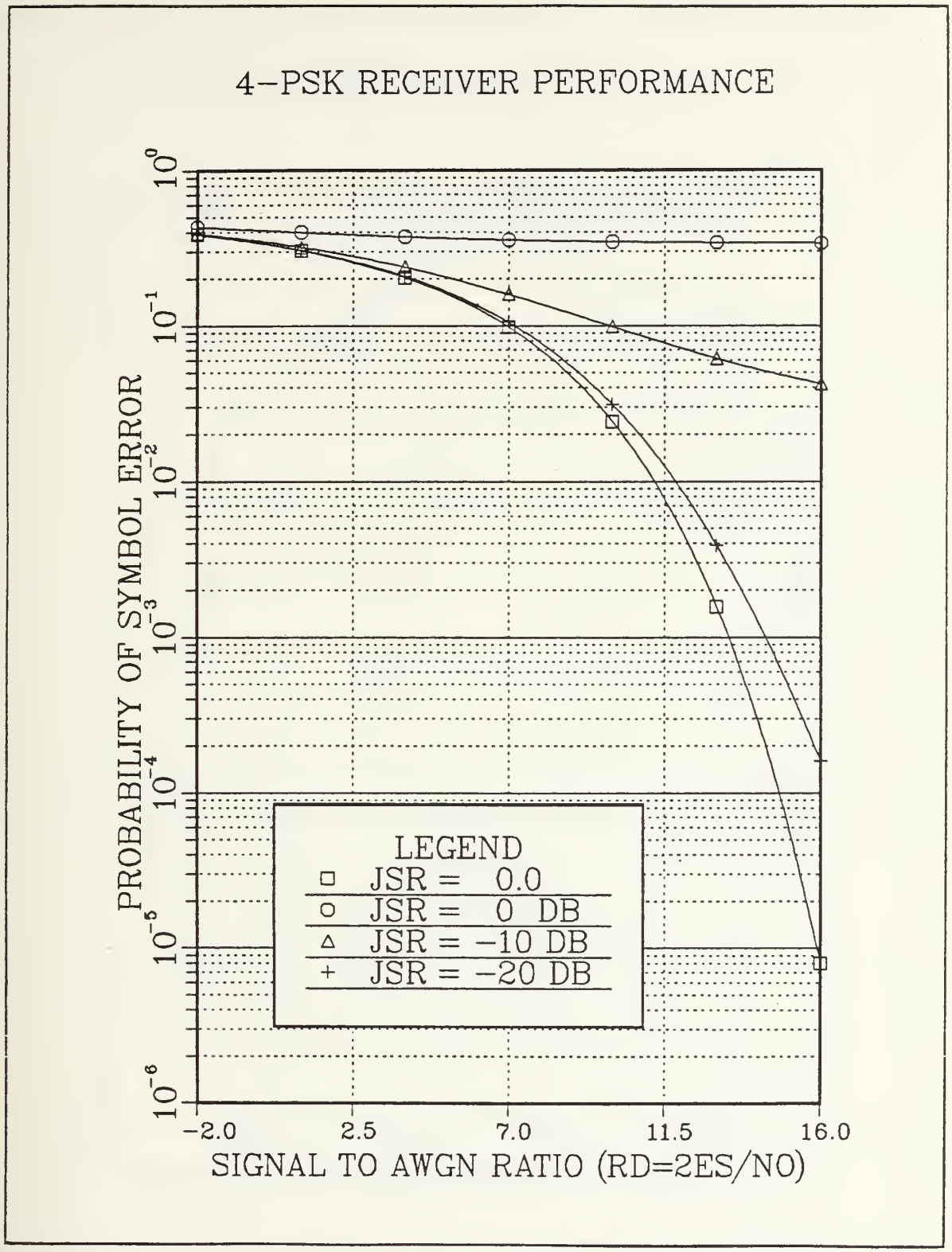

Figure 2.2 4-PSK Receiver Performance

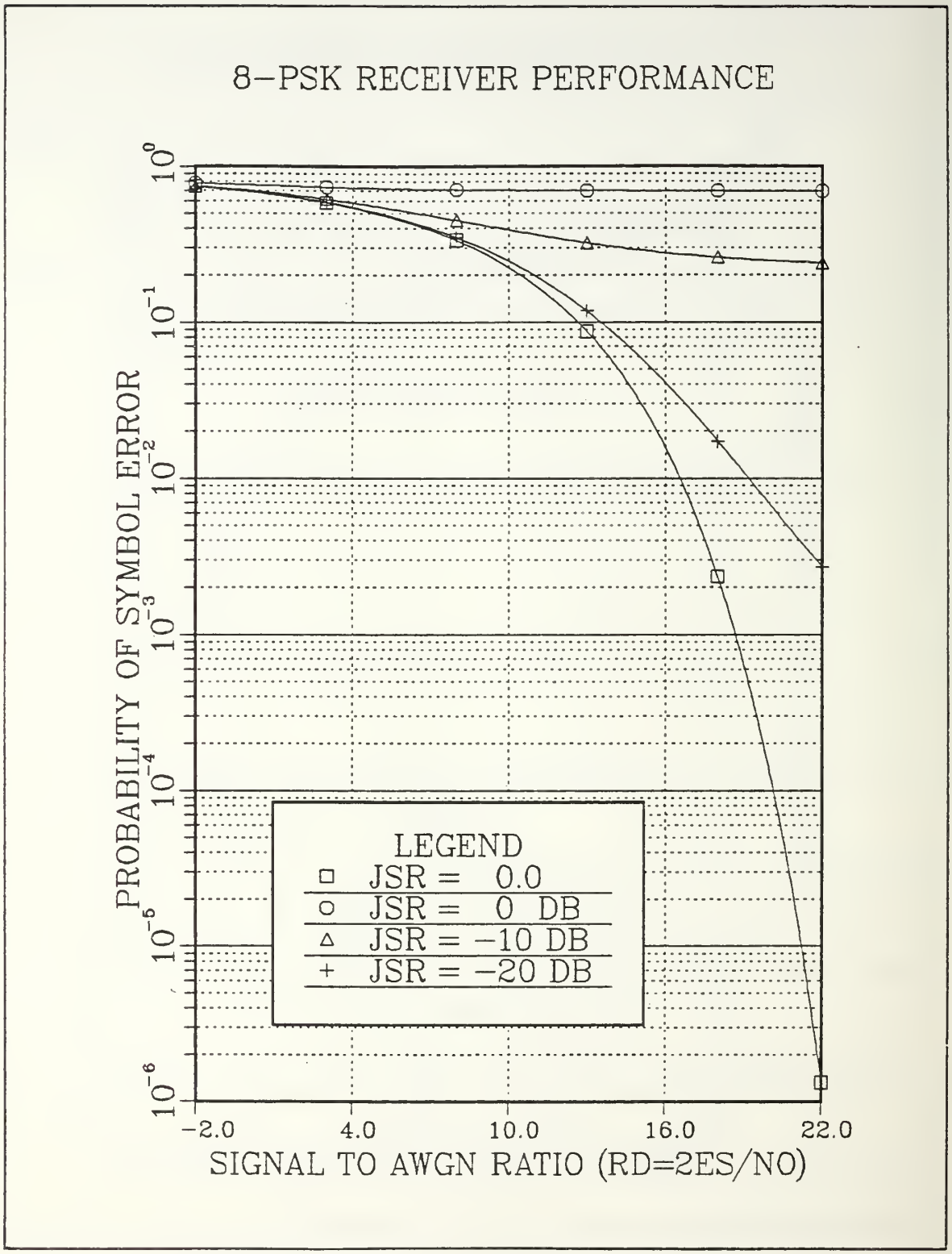

Figure 2.3 8-PSK Receiver Performance

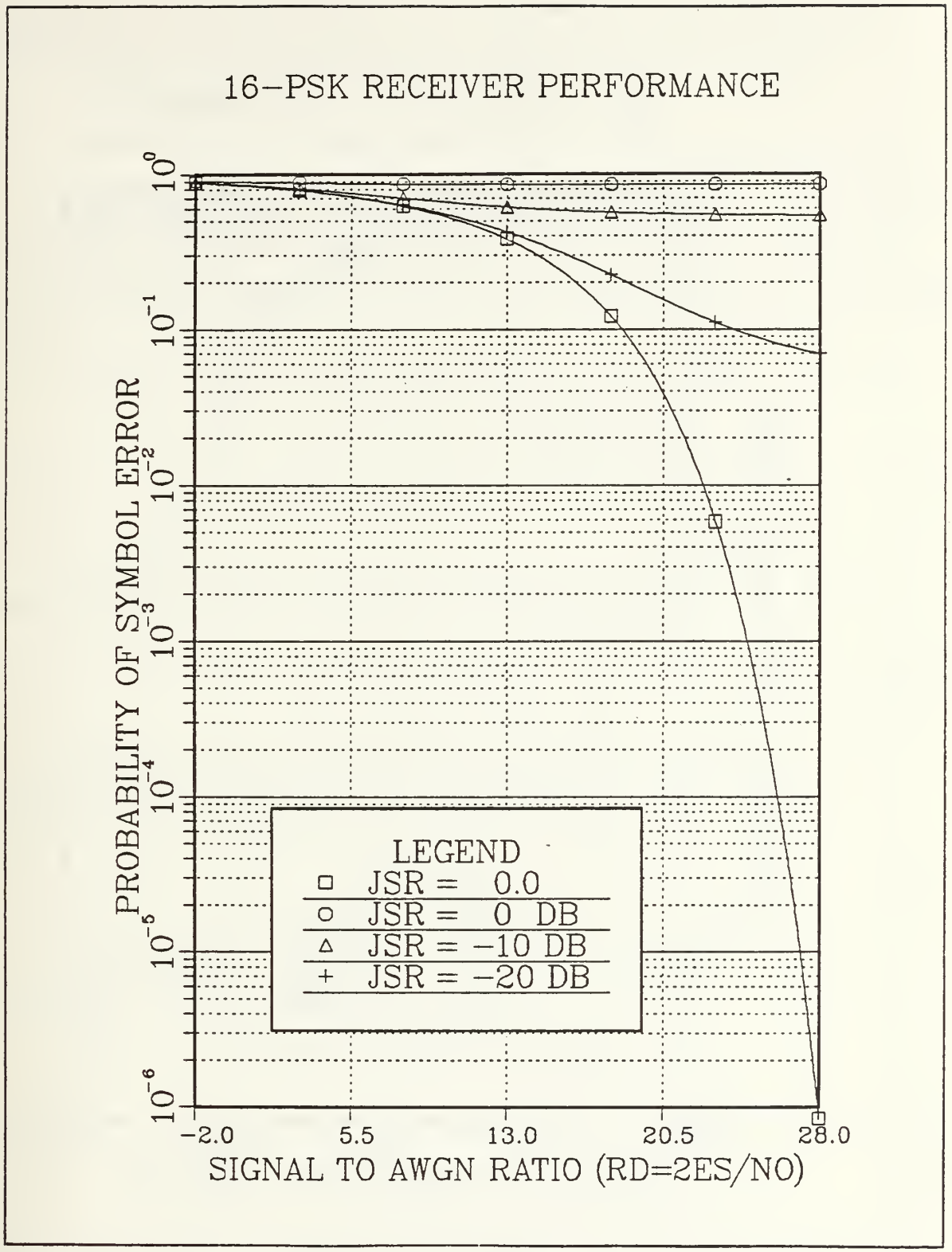

Figure 2.4 16-PSK Receiver Performance

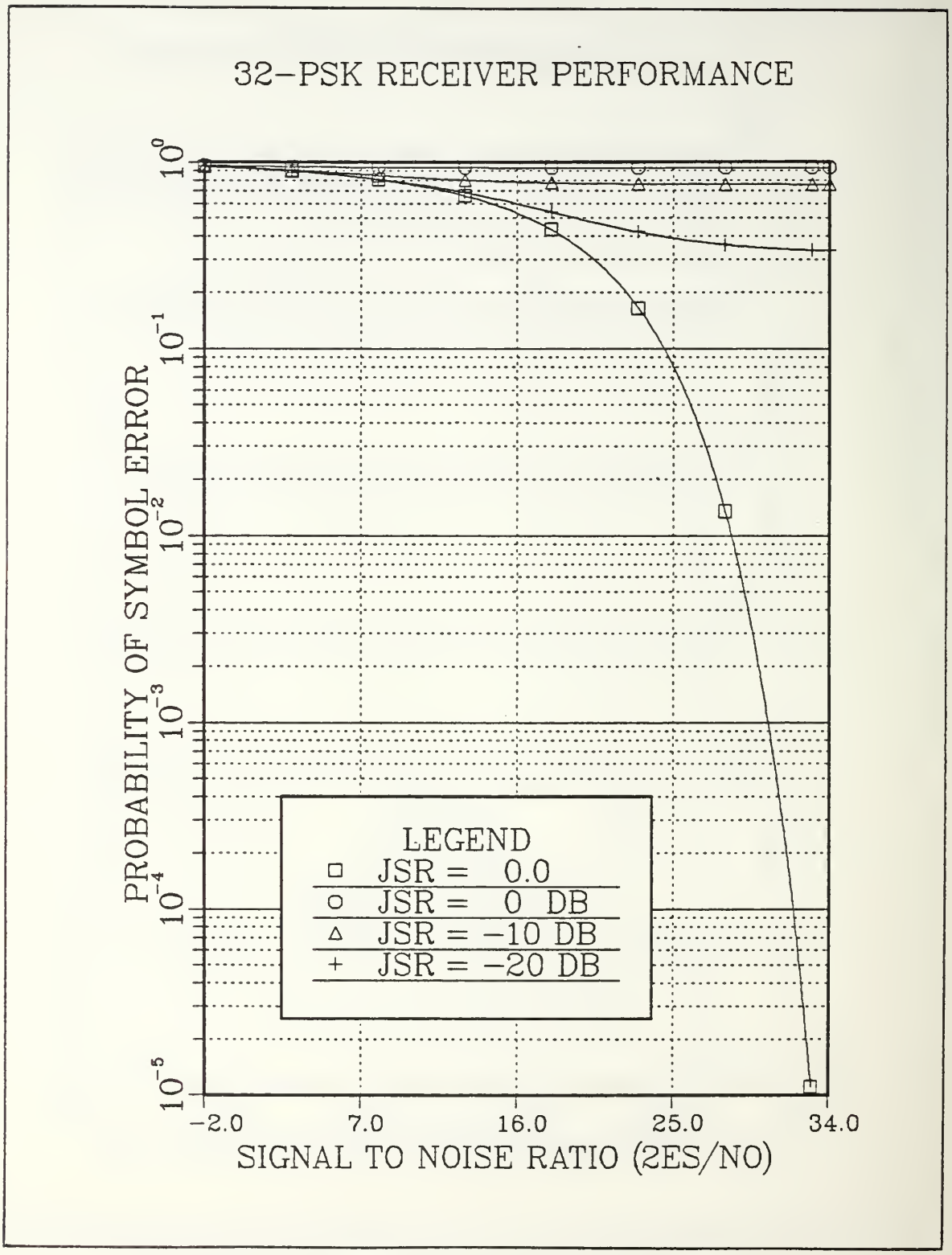

Figure 2.5 32-PSK Receiver Performance

cause maximum degradation to the receiver performance while maintaining power constrained conditions on the jammer.

B. OPTIMIZATION OF THE COLORED NOISE JAMMER

We now investigate the dependence of Pr{c} on the jamming to signal ratio, R_J, by analyzing the unsimplified form of Pr{c} given by equation (2.49) with equation (2.41) substituted for the conditional p.d.f., namely

$$\Pr\{c\} = 2\int_0^{\pi/M}\int_0^{\infty} \frac{x}{2\pi} \exp\{-\frac{1}{2}[x^2-2x\sqrt{R_D'}\cos\beta+R_D']\}dxd\beta \qquad (2.57)$$

where now

$$R_D' = \frac{E_s}{N_0/2 + \sigma_c^2} \qquad (2.58)$$

With the double change of variables

$$u = x\cos\beta \; ; \quad v = x\sin\beta \qquad (2.59)$$

equation (2.57) becomes

$$\Pr\{c\} = 2\int_0^{\infty} \frac{1}{\sqrt{2\pi}} \exp\{-\frac{1}{2}[u-\sqrt{R_D'}]^2\}\int_0^{u\tan\pi/M} \frac{1}{\sqrt{2\pi}} \exp\{-v^2/2\}dvdu \qquad (2.60)$$

We notice that in terms of R_D and R_J,

$$\sqrt{R_D'} = \sqrt{R_D/1+R_DR_J} \qquad (2.61)$$

Evaluating now the derivative of equation (2.60) with respect to R_J, we obtain

$$\frac{d}{dR_J} Pr\{c\} = -\frac{1}{2}\sqrt{\frac{R_D^3}{(1+R_D R_J)^3}} \int_0^\infty erf_*\{u\tan\pi/M\}$$

$$\times [u-\sqrt{R_D/1+R_D R_J}]\exp\{-\frac{1}{2}[u-\sqrt{R_D/1+R_D R_J}]^2\}du \qquad (2.62)$$

and with the change of variables

$$x = \frac{1}{2}[u - \sqrt{R_D/1+R_D R_J}]^2 \qquad (2.63)$$

we have

$$\frac{d}{dR_J} Pr\{c\} = -\frac{1}{2}\sqrt{\frac{R_D^3}{(1+R_D R_J)^3}} \int_{R_D/2(1+R_D R_J)}^\infty erf_*\{[\sqrt{2x}$$

$$+ \sqrt{R_D/1+R_D R_J}]\tan \pi/M\}e^{-x}\, dx \qquad (2.64)$$

Since both $erf_*\{x\}$ and e^{-x} are non-negative functions for all x, the integration in equation (2.64) must result in a non-negative quantity. Therefore,

$$\frac{d}{dR_J} Pr\{c\} < 0 \qquad (2.65)$$

which indicates that the probability of making a correct decision is a monotonically decreasing function with respect

to R_J. As a result, in order to maximize the detrimental effect of the jammer on the performance of the MPSK receiver, we will want to maximize the jamming power, within assumed power constrained limits.

Returning to equations (2.25) and (2.52), for a fixed signal energy, R_J can be maximized by maximizing

$$\sigma_c^2 = \int_{-\infty}^{\infty} S_c(f)|\Phi_1'(f)|^2 df \tag{2.66}$$

By the Cauchy-Schwartz inequality

$$\sigma_c^2 \leq \sqrt{\int_{-\infty}^{\infty} S_c^2(f)df \int_{-\infty}^{\infty} |\Phi_1'(f)|^4 df} \tag{2.67}$$

with equality if and only if

$$S_c(f) = K|\Phi_1'(f)|^2 \tag{2.68}$$

where K is an arbitrary constant. Since we require that the jamming signal be power constrained, that is

$$P_c = \int_{-\infty}^{\infty} S_c(f)df < \infty \tag{2.69}$$

then, provided that

$$\int_{-\infty}^{\infty} |\Phi_1'(f)|^2 df < \infty \tag{2.70}$$

we must select K such that the power constraint of equation (2.69) is satisfied.

For

$$\phi_1(t) = \sqrt{2/T_s}\cos[2\pi f_0 t+\alpha] \quad 0 \leq t \leq T_s \tag{2.71}$$

we can define

$$p(t) = \begin{cases} \sqrt{2/T_s} & 0 \leq t \leq T_s \\ 0 & \text{otherwise} \end{cases} \leftrightarrow P(f) = \sqrt{2T_s}\exp\{-j\pi f T_s\}\frac{\sin\pi f T_s}{\pi f T_s} \tag{2.72}$$

The Fourier Transform of $\cos[2\pi f_0 t+\alpha]$ is

$$\tfrac{1}{2}[\delta(f-f_0)+\delta(f+f_0)]\exp\{jf\alpha/f_0\} \tag{2.73}$$

so that

$$\Phi_1'(f) = \tfrac{1}{2}[P(f-f_0)+P(f+f_0)]\exp\{jf\alpha/f_0\} \leftrightarrow \phi_1'(t) \tag{2.74}$$

and

$$|\Phi_1'(f)|^2 = \tfrac{1}{4}[|P(f-f_0)|^2+|P(f+f_0)|^2+P(f-f_0)P^*(f+f_0)+P^*(f-f_0)P(f+f_0)] \tag{2.75}$$

The last two terms in equation (2.75) for reasonable values of carrier frequency, f_0, are negligible. Returning to equation (2.68), we now have

$$S_c(f) = \frac{K}{4}[|P(f-f_0)|^2 + |P(f+f_0)|^2] \tag{2.76}$$

and this results in

$$\int_{-\infty}^{\infty} S_c(f)df = K \tag{2.77}$$

Therefore

$$S_c(f) = P_c|\Phi_1'(f)|^2 \tag{2.78}$$

so that

$$\sigma_c^2 = \frac{1}{16} P_c \tag{2.79}$$

thus demonstrating that optimized jamming of an MPSK receiver requires in essence the spectrum of the colored noise jammer to be matched to the spectrum of the MPSK signal.

III. SPECIAL CASES OF COHERENT MPSK: QUADRATURE PHASE SHIFT KEYING, OFFSET QUADRATURE PHASE SHIFT KEYING AND MINIMUM SHIFT KEYING

Quadrature Phase Shift Keyed (QPSK) modulation is a special case of MPSK modulation where M = 4. Offset QPSK (OQPSK) is a special case of QPSK in which the in-phase and quadrature data components are offset in time by one-half of a symbol interval. Minimum Shift Keying (MSK) is furthermore a special case of OQPSK in which sinusoidal pulse weighting prior to carrier modulation produces a more compact signal spectrum making this modulation scheme very useful in cases where severe bandwidth constraints are imposed.

A. QPSK RECEIVER PERFORMANCE

The optimum receiver for a QPSK modulated signal is a special version of that shown in Figure 2.1 where now M = 4 and appropriate simplifications are made as shown in Figure 3.1.

Development of this receiver's performance from equation (2.53) with M = 4 is mathematically difficult and does not provide any significant insight to the results derived. Therefore, the QPSK receiver performance will be developed by relying on results presented in the previous chapter so as to be able to reduce the necessary development.

For the QPSK signaling scheme, the transmitted signals are as given by equation (2.1) of the form

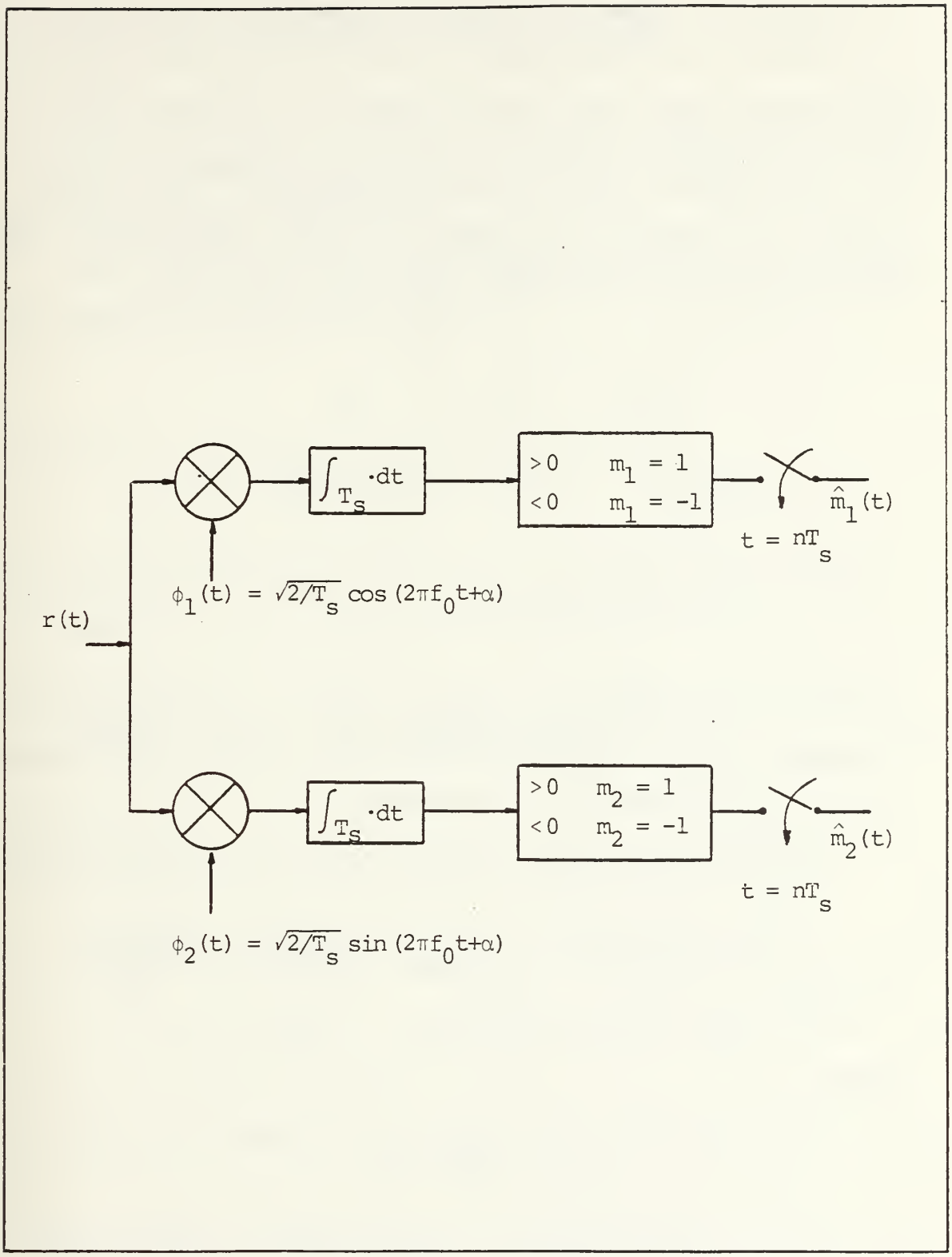

Figure 3.1 Optimum QPSK Receiver Structure

$$s_i(t) = \sqrt{2E_s/T_s}\cos\left[2\pi f_0 t + \frac{\pi(i-1)}{2} + \alpha\right] \quad i = 1,2,3,4 \qquad (3.1)$$

We will consider the case in which all signals $s_i(t)$, $i = 1,2,3,4$, are equally likely to be transmitted. The analysis begins by assuming that signal $s_1(t)$ was transmitted. Under this assumption, the statistics of Y_1 and Y_2 are

$$E\{Y_1\} = E\{Y_2\} = E_s \qquad (3.2)$$

$$Var\{Y_1\} = Var\{Y_2\} = \frac{N_0}{2} + \sigma_c^2 \qquad (3.3)$$

$$E\{[Y_1 - E\{Y_1\}][Y_2 - E\{Y_2\}]\} = 0 \qquad (3.4)$$

Just as in the MPSK case, both Y_1 and Y_2 are conditionally Gaussian random variables which, due to their uncorrelatedness, are statistically independent.

The joint probability density function of Y_1 and Y_2 is

$$f_{Y_1,Y_2|s_1(t)}(Y_1,Y_2|s_1(t)) = \frac{1}{2\pi\sigma^2}\exp\{-\frac{(Y_1-E_s)^2}{2\sigma^2}\}\exp\{-\frac{(Y_2-E_s)^2}{2\sigma^2}\} \qquad (3.5)$$

where

$$\sigma^2 = \frac{N_0}{2} + \sigma_c^2 \qquad (3.6)$$

In order to find the probability of making a correct decision conditioned on the assumption that signal $s_1(t)$ was

sent, we first examine the QPSK signal space diagram of Figure 3.2 so as to be able to determine this probability. For the QPSK case, the axes of the state space diagram serve as the perpendicular bisectors separating the decision regions associated with each signal.

Given that $s_1(t)$ was sent, the probability of the detector making a correct decision is

$$\Pr\{c|s_1(t)\} = \int_0^\infty \int_0^\infty f_{Y_1,Y_2|s_2(t)}(y_1,y_2|s_1(t))dY_1dY_2 \tag{3.7}$$

Evaluation of equation (3.7) using equation (3.5) yields the result

$$\Pr\{c|s_1(t)\} = [\text{erf}_*\{\sqrt{R_D/2(1+R_DR_J)}\}]^2 \tag{3.8}$$

where again

$$R_D = 2E_s/N_0: \text{ Signal to Noise Ratio (SNR)} \tag{3.9}$$

$$R_J = \sigma_c^2/E_s : \text{ Jamming to Signal Ratio (JSR)} \tag{3.10}$$

A similar development for $s_2(t)$, $s_3(t)$ and $s_4(t)$ results in

$$\Pr\{c|s_1(t)\} = \Pr\{c|s_2(t)\} = \Pr\{c|s_3(t)\} = \Pr\{c|s_4(t)\} \tag{3.11}$$

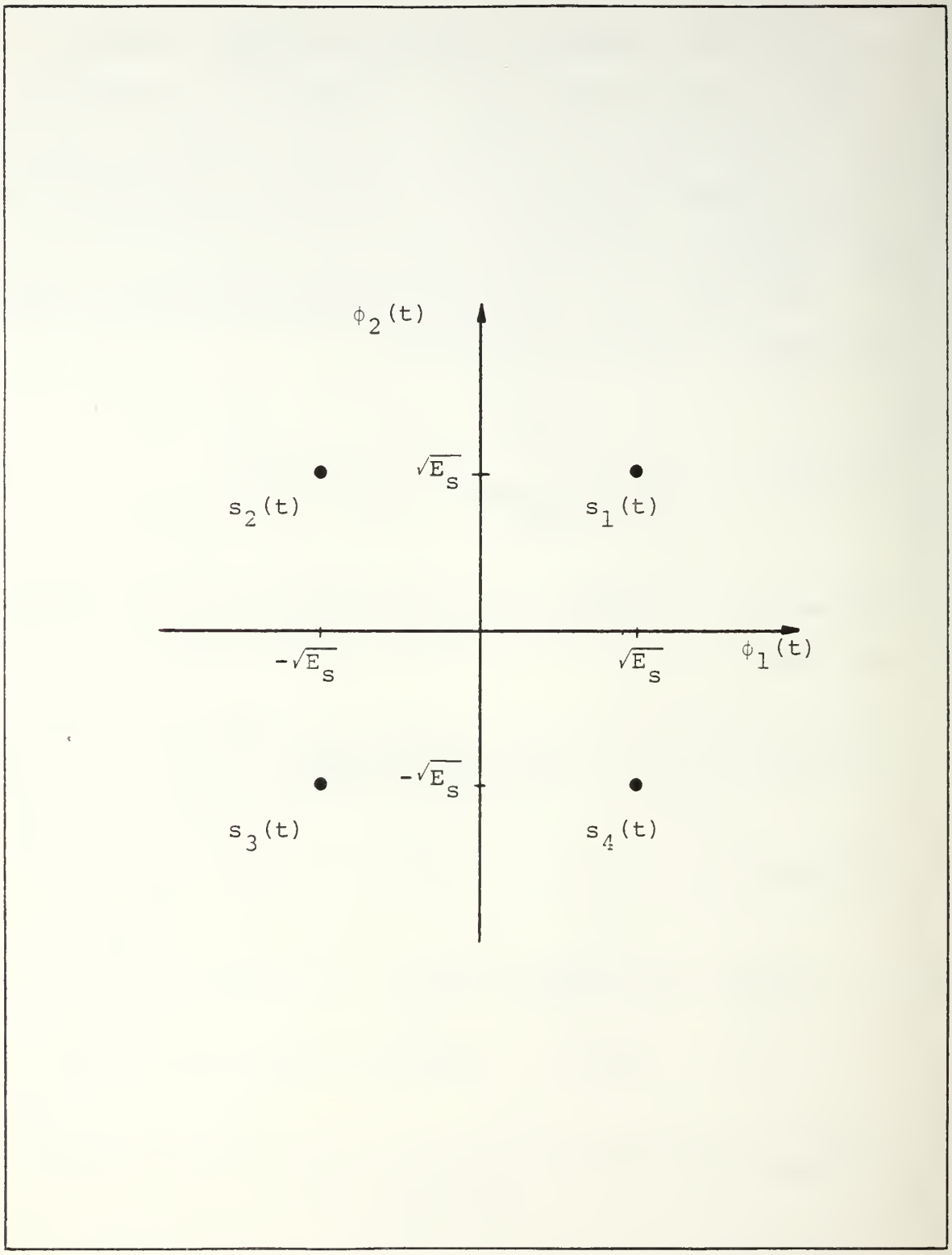

Figure 3.2 Signal Space Diagram for QPSK Signaling

and therefore, since all signals are assumed equally likely

$$\Pr\{c\} = [\mathrm{erf}_*\{\sqrt{R_D/2(1+R_D R_J)}\}]^2 = 1 - \Pr\{\varepsilon\} \tag{3.12}$$

Observe that if the colored noise is not present, $R_J = 0$, $\sigma^2 = N_0/2$ and equation (3.12) becomes

$$\Pr\{c\} = [\mathrm{erf}_*\{\sqrt{E_s/N_0}\}]^2 \tag{3.13}$$

which is the probability of making a correct decision for a QPSK modulated signal transmitted over a channel corrupted by AWGN.

Furthermore, if the jamming power grows without bound,

$$\lim_{R_J \to \infty} \Pr\{c\} = \frac{1}{4} \tag{3.14}$$

which is as expected the minimum value of the probability of a correct decision for a set of 4 equiprobable signals.

The optimization of the jammer is identical to that derived for MPSK signaling and as such, the spectrum of the optimum colored noise jammer is given by

$$S_c(f) = P_c |\Phi_1'(f)|^2 \tag{3.15}$$

where

$$\sigma_c^2 = \frac{1}{16} P_c \tag{3.16}$$

The corresponding probability of symbol error is plotted in Figure 3.3 as a function of SNR for various jamming-to-signal power ratios.

B. OFFSET QPSK RECEIVER PERFORMANCE

QPSK signaling techniques as previously pointed out are attractive from a bandwidth efficiency point of view. For an unfiltered QPSK signal, phase transitions occur instantaneously resulting in a constant amplitude envelope signal. However, phase changes for filtered QPSK signals result in a varying envelope amplitude. Offset QPSK signaling, in which the in-phase and quadrature data bits are offset or staggered by one-half of a symbol interval results in a more constant amplitude envelope even after filtering. When a bandlimited offset QPSK signal is transmitted through an amplitude-limiting device, there is only partial regeneration of the spectrum amplitude back to the unfiltered level. For QPSK under the same circumstances, however, there is almost complete regeneration to the unfiltered level. [Ref. 3]

Figure 3.4 shows the structure of the optimum offset QPSK receiver.

Since offset QPSK uses the same principles, waveforms and receiver structure as those used in QPSK with the exception that now, one channel is offset in time with respect to the other one by one-half of a symbol interval, it should not be surprising to find that the performance of the receiver of Figure 3.4, with or without jamming is identical to that of

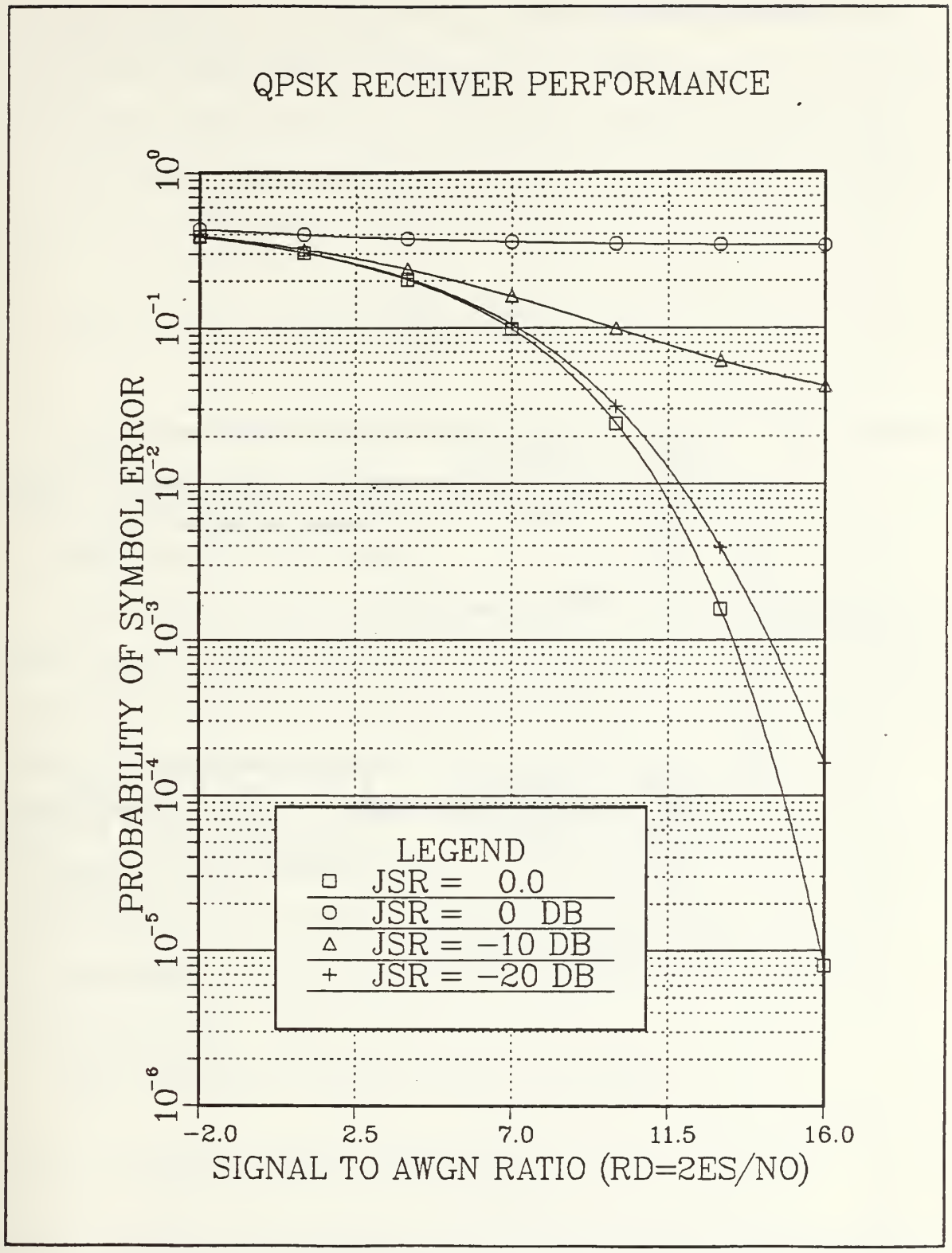

Figure 3.3 QPSK Receiver Performance

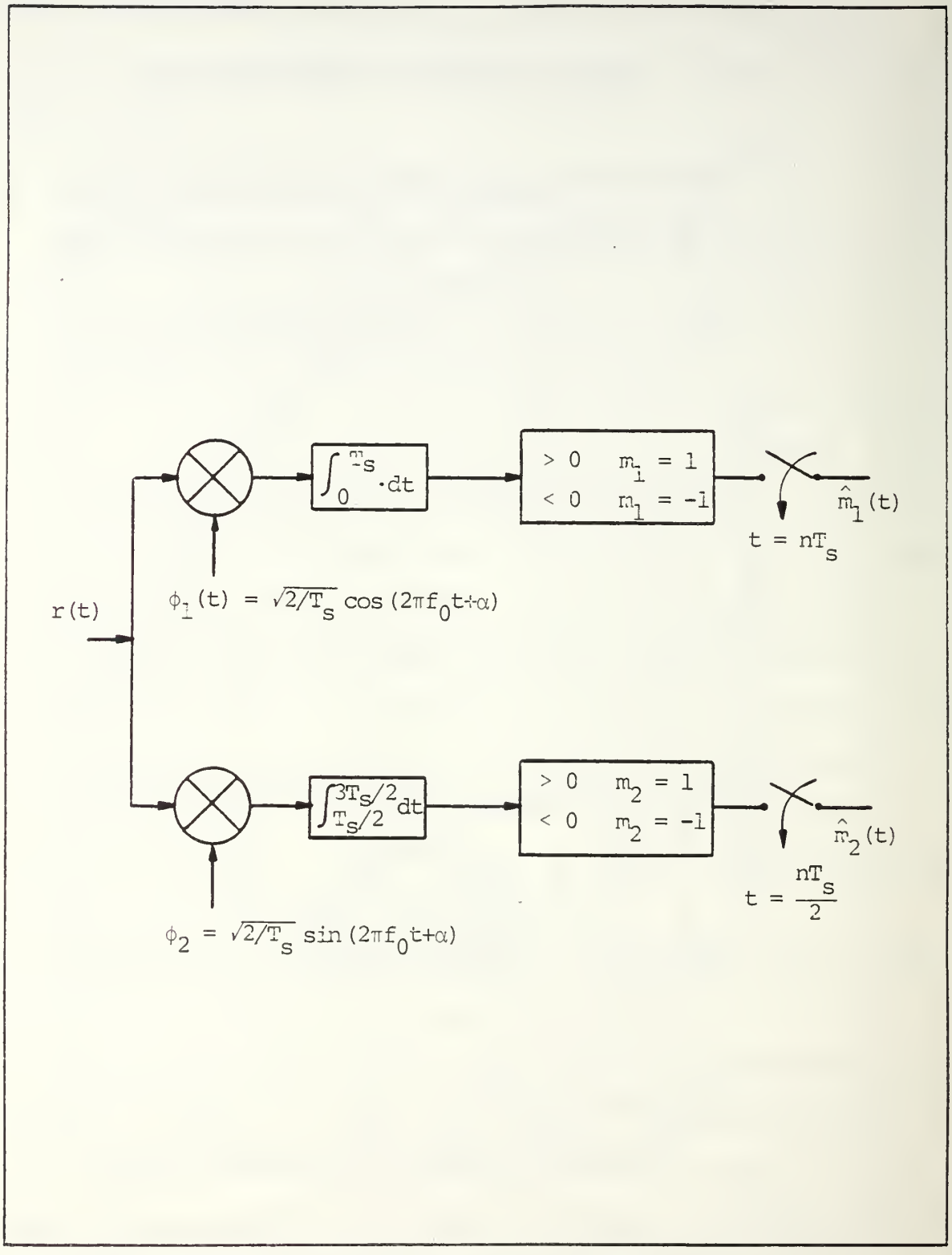

Figure 3.4 Optimum Offset QPSK Receiver Structure

the QPSK receiver of Figure 3.1. The only difference is that the offset QPSK receiver operates on delayed data so that one correlator must offset its integration interval accordingly.

Therefore, the probability of error is as given in equation (3.12), namely

$$Pr\{\varepsilon\} = 1 - [erf_{*}\{\sqrt{R_D/2(1+R_D R_J)}\}]^2 \qquad (3.17)$$

and the corresponding performance curves are obviously identical to those shown in Figure 3.3.

C. MSK RECEIVER PERFORMANCE

The logical progression from QPSK to offset QPSK suggests that further suppression of out-of-band interference in band-limiting applications can be obtained if the offset QPSK signal format is modified to avoid phase transitions altogether. Minimum Shift Keying (MSK) is a constant envelope modulation with continuous phase at the bit transition times which provides the desired sideband suppression. The MSK signal can be considered to be an offset QPSK signal with sinusoidal pulse weighting. [Ref. 4]

The transmitted signals are of the form

$$s_i(t) = \sqrt{2E_s/T_s}\, a_I(t)\cos(2\pi f_1 t)\cos[2\pi f_0 t+\alpha]$$

$$+ \sqrt{2E_s/T_s}\, a_Q(t)\sin(2\pi f_1 t)\sin[2\pi f_0 t+\alpha] \qquad i = 1,2,3,4 \qquad (3.18)$$

where $a_I(t)$ and $a_Q(t)$ are the in-phase and quadrature binary data. The orthonormal basis functions necessary to represent the MSK signals as an equivalent orthogonal series now take on the form

$$\phi_1(t) = \sqrt{4/T_s}\cos(2\pi f_1 t)\cos[2\pi f_0 t+\alpha] \; ; \qquad (3.19)$$

$$\phi_2(t) = \sqrt{4/T_s}\sin(2\pi f_1 t)\sin[2\pi f_0 t+\alpha]$$

The optimum receiver for the recovery of the MSK signals is shown in Figure 3.5.

Assuming that all signals $s_i(t)$, $i = 1,2,3,4$ are equally likely to be transmitted and given a priori knowledge that signal $s_1(t)$ was transmitted, the received signal is

$$r(t) = s_1(t) + n_w(t) + n_c(t) \qquad (3.20)$$

where again $n_w(t)$ is a sample function of a white Gaussian noise process with zero mean and two-sided power spectral density level $N_0/2$ watts/Hz, and $n_c(t)$ is a sample function of a colored Gaussian noise process having autocorrelation function $K_c(\tau)$.

The statistics of Y_1 and Y_2 are given by

$$E\{Y_1|s_1(t)\} = E\{Y_2|s_1(t)\} = E_s \qquad (3.21)$$

$$\mathrm{Var}\{Y_1|s_1(t)\} = E\{n_{w_1}^2\} + E\{n_{c_1}^2\} \qquad (3.22)$$

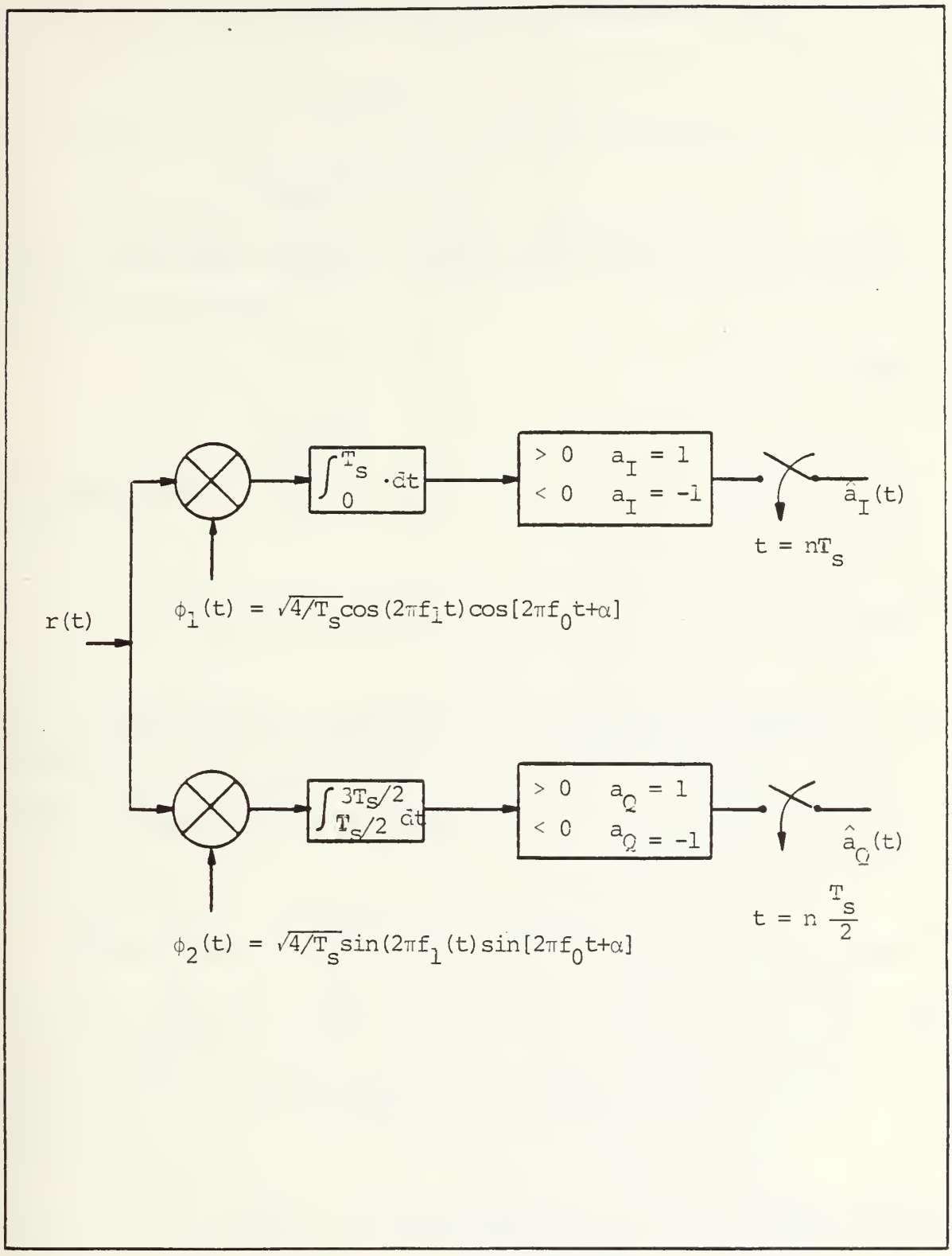

Figure 3.5 Optimum MSK Receiver Structure

$$\text{Var}\{Y_2|s_1(t)\} = E\{n_{w_2}^2\} + E\{n_{c_2}^2\} \tag{3.23}$$

where

$$n_{w_1} = \int_0^{T_s} n_w(t)\phi_1(t)dt \; ; \quad n_{w_2} = \int_{T_s/2}^{3T_s/2} n_w(t)\phi_2(t)dt \tag{3.24}$$

and

$$n_{c_1} = \int_0^{T_s} n_c(t)\phi_1(t)dt \; ; \quad n_{c_2} = \int_{T_s/2}^{3T_s/2} n_c(t)\phi_2(t)dt \tag{3.25}$$

Also

$$E\{[Y_1-E\{Y_1\}][Y_2-E\{Y_2\}]\} = E\{n_{w_1}n_{w_2}\} + E\{n_{c_1}n_{c_2}\} \tag{3.26}$$

Evaluating the first term in equation (3.26) yields

$$E\{n_{w_1}n_{w_2}\} = E\left\{\int_0^{T_s} n_w(t)\phi_1(t)dt \int_{T_s/2}^{3T_s/2} n_w(\tau)\phi_2(\tau)d\tau\right\}$$

$$= \int_{T_s/2}^{T_s} \frac{N_0}{2}\phi_1(t)\phi_2(t)dt = 0 \tag{3.27}$$

From this result we observe that

$$E\{n_{w_1}^2\} = E\{n_{w_2}^2\} = \frac{N_0}{2} \tag{3.28}$$

The second term in equation (3.26) leads to

$$E\{n_{c_1} n_{c_2}\} = \int_0^{T_s} \int_{T_s/2}^{3T_s/2} K_c(t-\tau)\phi_1(t)\phi_2(\tau)dt\, d\tau \qquad (3.29)$$

Using techniques similar to those used in the MPSK case, it can be shown that

$$E\{n_{c_1} n_{c_2}\} = 0 \qquad (3.30)$$

Therefore

$$E\{[Y_1-E\{Y_1\}][Y_2-E\{Y_2\}]\} = 0 \qquad (3.31)$$

so that the remaining analysis for the performance of the MSK receiver is identical to that of the QPSK receiver. Therefore, the probability of a symbol error is

$$Pr\{\varepsilon\} = 1 - [erf_*\{\sqrt{R_D/2(1+R_D R_J)}\}]^2 \qquad (3.32)$$

and the spectrum of the optimum colored noise jammer has the same mathematical form as that of MPSK, QPSK and OQPSK, namely

$$S_c(f) = P_c|\Phi_1'(f)|^2 \qquad (3.33)$$

except that now, due to the modification of $\phi_1(t)$ as indicated by equation (3.19), the spectrum of the colored noise jammer is given by

$$S_c(f) = P_c|\Phi_1'(f)|^2 = \frac{4P_cE_s}{\pi^2}\left[\frac{\cos^2\pi(f-f_0)T_s}{[1-(2(f-f_0)T_s)^2]^2} + \frac{\cos^2\pi(f+f_0)T_s}{[1-(2(f+f_0)T_s)^2]^2}\right] \tag{3.34}$$

as opposed to the spectrum of the colored noise jammer for QPSK given by

$$S_c(f) = P_c|\Phi_1'(f)| = \frac{E_sP_c}{2}\left[\left(\frac{\sin\pi(f-f_0)T_s}{\pi(f-f_0)T_s}\right)^2 + \left(\frac{\sin\pi(f+f_0)T_s}{\pi(f+f_0)T_s}\right)^2\right] \tag{3.35}$$

IV. DIFFERENTIALLY COHERENT PHASE SHIFT KEYING

Differentially Coherent Phase Shift Keying (DPSK) is a signaling technique which eliminates the need for phase synchronization of the local carrier to the received signal by using a delayed version of the received signal as the local reference during demodulation. At the transmitter, the digital information is encoded into phase differences between two successive signaling intervals and then modulated onto the carrier using conventional PSK techniques. DPSK allows the use of simpler and therefore less costly receiver structures at the expense of only a slight performance degradation as compared to coherent PSK signaling. [Ref. 5]

A. DPSK RECEIVER PERFORMANCE IN COLORED NOISE JAMMING

Contrasted to the coherent signaling techniques previously analyzed, DPSK analysis poses a mathematically formidable task, even in the case of binary signaling over an AWGN corrupted channel. Consequently, the evaluation of the receiver performance will use the geometric approach first developed by Arthurs and Dym [Ref. 6], extended here to the case where the channel interference consists of additional colored noise jamming.

The signal set for DPSK signaling is identical to that for MPSK signaling as given by equation (2.1). Define T_i to be the i^{th} signaling interval so that $t \in T_i \rightarrow (i-1)T_s \leq t \leq iT_s$,

$i = 1,2,\ldots$. The transmitted DPSK signals are therefore given by

$$s(t) = \sqrt{2E_s/T_s}\cos[2\pi f_0 t + \theta^{(i)} + \alpha], \quad t \in T_i \tag{4.1}$$

where

$$\theta^{(i)} = \theta^{(i-1)} + \theta_\ell \quad \text{(modulo } 2\pi) \tag{4.2}$$

The phase information is denoted by θ_ℓ and α is an arbitrary, yet fixed phase. The possible values that $\theta^{(i)}$ can take on are

$$\theta^{(i)} = \frac{2\pi(j-1)}{M} \qquad j = 1,2,\ldots,M \tag{4.3}$$

The optimum receiver structure for such a signaling scheme is shown in Figure 4.1. In Figure 4.1, β represents the receiver phase ambiguity. In much the same way as in noncoherent demodulation, no attempt is made to phase lock the receiver in such a way that $\beta = \alpha$.

The received signal is

$$r(t) = s(t) + n_w(t) + n_c(t), \quad t \in T_i \tag{4.4}$$

where the noise components are the same as those used in previous analyses.

In order to evaluate the DPSK receiver performance, the probability density function of $\eta^{(i)}$ must be found. To this end, the statistics of Y_1 and Y_2 are required.

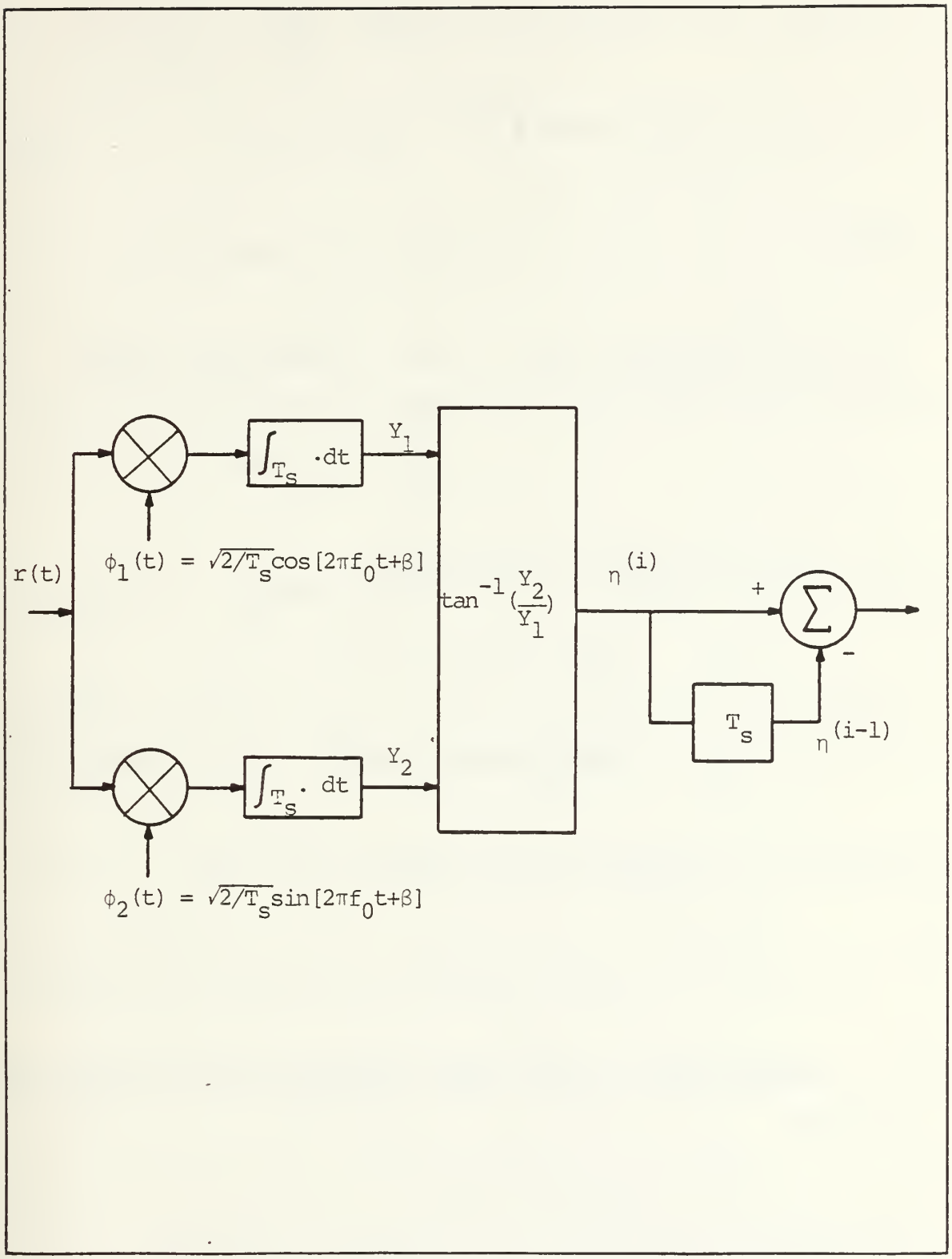

Figure 4.1 Optimum DPSK Receiver Structure

$$Y_1 = \sqrt{E_s}\cos[\alpha-\beta+\theta^{(i)}] + n_{w_1} + n_{c_1} \tag{4.5}$$

$$Y_2 = -\sqrt{E_s}\sin[\alpha-\beta+\theta^{(i)}] + n_{w_2} + n_{c_2} \tag{4.6}$$

where

$$n_{w_j} = \int_0^{T_s} n_w(t)\phi_j(t)dt \; ; \quad n_{c_j} = \int_0^{T_s} n_c(t)\phi_j(t)dt \tag{4.7}$$

$$j = 1,2$$

The expected value of Y_1 and Y_2 is

$$E\{Y_1\} = \sqrt{E_s}\cos[\phi_e + \theta^{(i)}] \tag{4.8}$$

$$E\{Y_2\} = -\sqrt{E_s}\sin[\phi_e + \theta^{(i)}] \tag{4.9}$$

where ϕ_e is the phase error defined by

$$\phi_e \triangleq \alpha - \beta \tag{4.10}$$

As shown for the MPSK case, a similar result holds here in that

$$E\{[Y_1-E\{Y_1\}][Y_2-E\{Y_2\}]\} = E\{n_{w_1} n_{w_2}\} + E\{n_{c_1} n_{c_2}\} = 0 \tag{4.11}$$

so that

$$\sigma_{Y_1}^2 = \sigma_{Y_2}^2 = \frac{N_0}{2} + \sigma_c^2 = \sigma^2 \tag{4.12}$$

and

$$E\{[Y_1-E\{Y_1\}][Y_2-E\{Y_2\}]\} = 0 \tag{4.13}$$

Again we find that Y_1 and Y_2 are independent Gaussian random variables and therefore, the joint probability density function of Y_1 and Y_2 is

$$f_{Y_1,Y_2}(Y_1,Y_2) = \frac{1}{2\pi\sigma^2}\exp\left\{-\frac{1}{2}\left[\frac{(Y_1-E\{Y_1\})^2}{\sigma^2} + \frac{(Y_2-E\{Y_2\})^2}{\sigma^2}\right]\right\} \tag{4.14}$$

In order to obtain the p.d.f. of $\eta^{(i)}$ we will use a double transformation of random variables, namely

$$V^{(i)} = \sqrt{Y_1^2 + Y_2^2}\ ; \quad \eta^{(i)} = \tan^{-1}(Y_2/Y_1) \tag{4.15}$$

resulting in a joint p.d.f. for $V^{(i)}$ and $\eta^{(i)}$ given by

$$f_{V^{(i)},H^{(i)}}(v,\eta) = vf_{Y_1Y_2}(v\cos\eta, v\sin\eta) + vf_{Y_1Y_2}(-v\cos\eta, -v\sin\eta) \tag{4.16}$$

$$v \geq 0; \quad 0 \leq \eta \leq \pi$$

from the p.d.f. of equation (4.14) we obtain

$$f_{V^{(i)},H^{(i)}}(v,\eta) = \frac{v}{2\pi\sigma^2}\exp\{-\frac{1}{2\sigma^2}[v^2-2v\sqrt{E_s}\cos[\eta+\phi_e+\theta^{(i)}]+E_s]\}$$

$$+ \frac{v}{2\pi\sigma^2}\exp\{-\frac{1}{2\sigma^2}[v^2-2v\sqrt{E_s}\cos[\eta+\phi_e+\theta^{(i)}+\pi]+E_s]\} \qquad (4.17)$$

$$v \geq 0; \quad 0 \leq \eta \leq \pi$$

Since the second term in equation (4.17) is equivalent to the first with the exception of the π radian offset, it is possible to eliminate the second term by allowing η to range from 0 to 2π. Thus

$$f_{V^{(i)},H^{(i)}}(v,\eta) = \frac{v}{2\pi\sigma^2}\exp\{-\frac{1}{2\sigma^2}[v^2-2v\sqrt{E_s}\cos[\eta+\phi_e+\theta^{(i)}]+E_s\} \qquad (4.18)$$

$$v \geq 0; \quad 0 \leq \eta \leq 2\pi$$

The p.d.f. of η is now obtained by integrating equation (4.18) over the range of V, namely

$$f_{H^{(i)}}(\eta) = \int_0^\infty f_{V^{(i)},H^{(i)}}(v,\eta)dv \qquad (4.19)$$

This integration leads to the result

$$f_{H^{(i)}}(\eta) = \frac{1}{2\pi}\exp\{\frac{-E_s\sin^2\psi}{2\sigma^2}\}[\exp\{\frac{-E_s\cos^2\psi}{2\sigma^2}\}$$

$$+ \sqrt{2\pi E_s/\sigma^2}\cos\psi\ \mathrm{erf}_*\{\sqrt{E_s/\sigma^2}\cos\psi\}] \qquad (4.20)$$

where

$$\psi = \eta + \phi_e + \theta^{(i)} \tag{4.21}$$

and

$$\sigma^2 = \frac{N_0}{2} + \sigma_c^2 \tag{4.22}$$

A similar expression is valid for the p.d.f. of $\eta^{(i-1)}$.

In order to obtain the probability of error performance of the DPSK receiver, it is necessary to evaluate

$$Pr\{\varepsilon\} = Pr\{|\eta^{(i)}-\eta^{(i-1)}-(\theta^{(i)}-\theta^{(i-1)})| > \pi/M\} \tag{4.23}$$

First, observe that as long as ϕ_e remains constant over two consecutive bit intervals, the mathematical expression of equation (4.23) remains unchanged so that it is possible to set $\phi_e = 0$ without loss of generality. Furthermore, for the binary case with equally likely signals $\theta^{(i)}-\theta^{(i-1)} = 0$ and $\theta^{(i)}-\theta^{(i-1)} = \pi$ each with probability 0.5.

Therefore it is necessary to only compute

$$Pr\{\varepsilon\} = Pr\{|\eta^{(i)}-\eta^{(i-1)}| > \pi/2\} \tag{4.24}$$

however it must be remembered that by considering only $\theta^{(i)}-\theta^{(i-1)} = 0$, two cases are in fact being analyzed, namely

$\theta^{(i)}-\theta^{(i-1)} = 0$ or $\theta^{(i)}-\theta^{(i-1)} = \pi$. Regardless of which of these cases occurs, the behavior of the angle $\eta^{(i)}-\eta^{(i-1)}$ remains unchanged. Since these two cases occur with the same probability, we assume without loss of generality that $\theta^{(i)}-\theta^{(i-1)} = 0$.

Figure 4.2 shows a typical signal space representation of received DPSK signals.

Assuming that $\eta^{(i-1)}$ is known, Figure 4.2 shows a line perpendicular to the vector corresponding to the assumed phase $\eta^{(i-1)}$, in order to highlight the region where the next received vector could lie and result in no receiver error.

In each case we have the vector $\sqrt{E_s}\underline{\phi}_1$ transmitted and a noise vector $\underline{n} = \underline{n}_w + \underline{n}_c$ added to it to form the corresponding received vector. The statistics of $\underline{n}$ are

$$E\{\underline{n}\} = 0 \tag{4.25}$$

$$\text{Var}\{\underline{n}\} = \frac{N_0}{2} + \sigma_c^2 \tag{4.26}$$

A receiver error will be made if the component of $\underline{n}$ along $\tilde{\underline{\phi}}_1$ exceeds $\sqrt{E_s}\cos\eta^{(i-1)}$. Since $\underline{n}$ is a Gaussian vector, regardless of the coordinate system chosen, the components of the noise along dimensions $\tilde{\phi}_1$ and $\tilde{\phi}_2$ will be zero mean, independent with variance σ^2 where

$$\sigma^2 = \frac{N_0}{2} + \sigma_c^2 \tag{4.27}$$

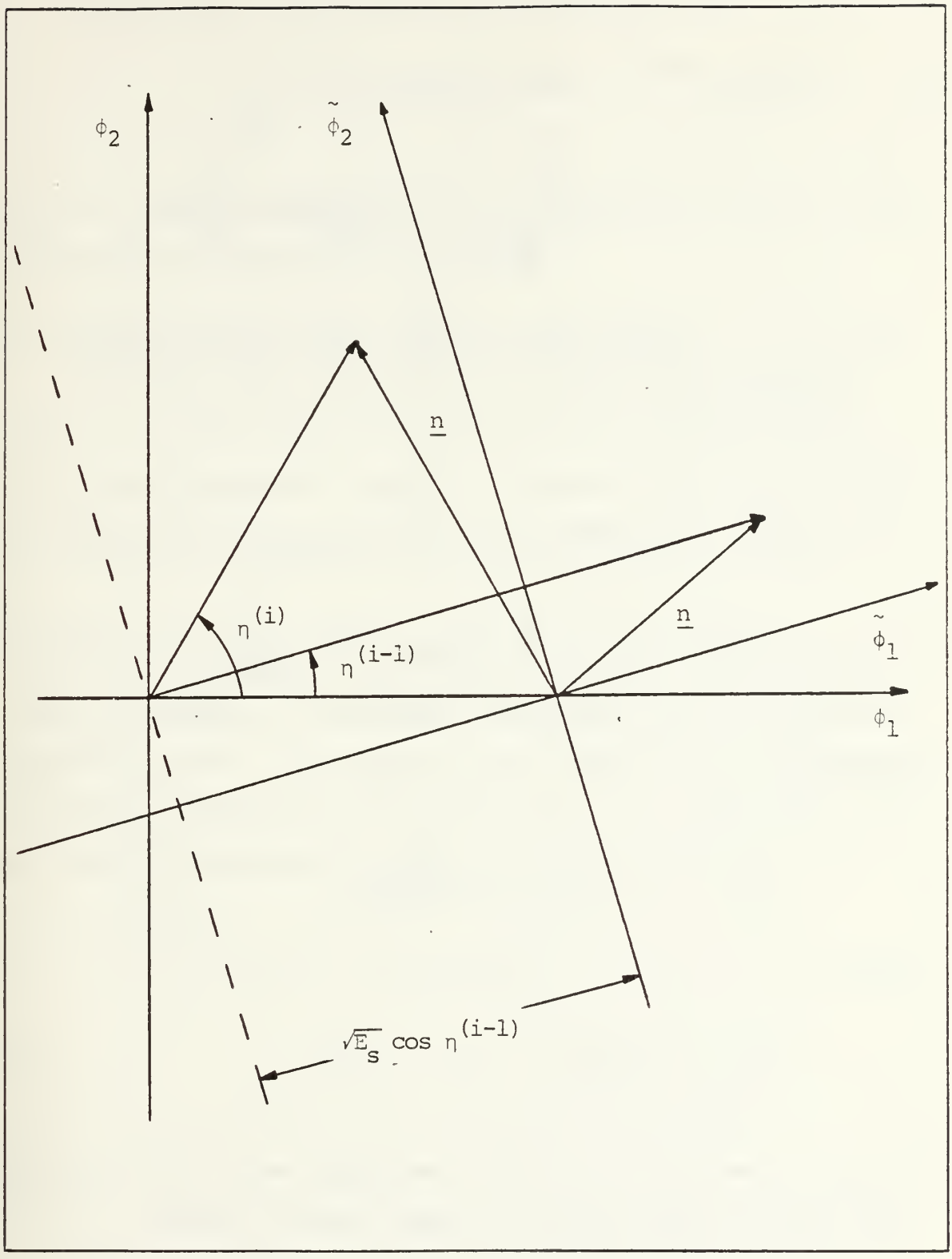

Figure 4.2 Signal Space Representation of Received DPSK Signals

Consequently

$$\Pr\{\text{Error}|\eta^{(i-1)}\} = \Pr\{\tilde{n}_1 > \sqrt{E_s}\cos\eta^{(i-1)}\}$$

$$= \int_{\sqrt{E_s}\cos\eta^{(i-1)}}^{\infty} \frac{1}{\sqrt{2\pi\sigma^2}} \exp\{-\frac{\tilde{n}_1^2}{2\sigma^2}\}d\tilde{n}_1 \qquad (4.28)$$

where $\tilde{n}_1$ is the component of the noise vector $\underline{n}$ along $\tilde{\phi}_1$.

Furthermore

$$\Pr\{\varepsilon\} = \int_{-\infty}^{\infty} \Pr\{\text{Error}|\eta^{(i-1)}\} f_{H(i-1)}(\eta^{(i-1)})d\eta^{(i-1)} \qquad (4.29)$$

Using the p.d.f. of $\eta^{(i-1)}$, with $\phi_e = 0$ and $\theta^{(i-1)} = 0$, carrying out the integration indicated in equation (4.29) yields

$$\Pr\{\varepsilon\} = \frac{1}{2}\exp\{-\frac{R_D}{2(1+R_D R_J)}\} \qquad (4.30)$$

where

$$R_D = 2E_s/N_0 \; ; \quad R_J = \sigma_c^2/E_s \qquad (4.31)$$

Observe that if no colored noise is present, the performance of a binary DPSK receiver in AWGN results, namely

$$\Pr\{\varepsilon\} = \frac{1}{2}\exp\{-\frac{E_s}{N_0}\} \qquad (4.32)$$

Furthermore, if R_J becomes infinitely large

$$\lim_{R_J \to \infty} \Pr\{\varepsilon\} = \frac{1}{2} \tag{4.33}$$

which is to be expected for a binary signaling scheme with equiprobable signals.

B. OPTIMIZATION OF THE COLORED NOISE JAMMER

Analyzing again the problem of designing an optimum jammer which will cause the greatest performance degradation to the DPSK receiver subject to a power constraint, we begin by taking derivatives of equation (4.30) with respect to R_J

$$\frac{d}{dR_J} \Pr\{\varepsilon\} = \frac{R_D^2}{4(1+R_D R_J)^2} \exp -\{\frac{R_D}{2(1+R_D R_J)}\} \geq 0 \quad \text{for all } R_J \tag{4.34}$$

Therefore, $\Pr\{\varepsilon\}$ is a monotonically increasing function with respect to the jamming-to-signal ratio, R_J. Therefore, just as for MPSK signaling

$$S_c(f) = P_c |\Phi_1'(f)|^2 \tag{4.35}$$

and

$$\sigma_c^2 = \frac{1}{16} P_c \tag{4.36}$$

The resulting DPSK receiver performance is plotted in Figure 4.3 for different values of R_J.

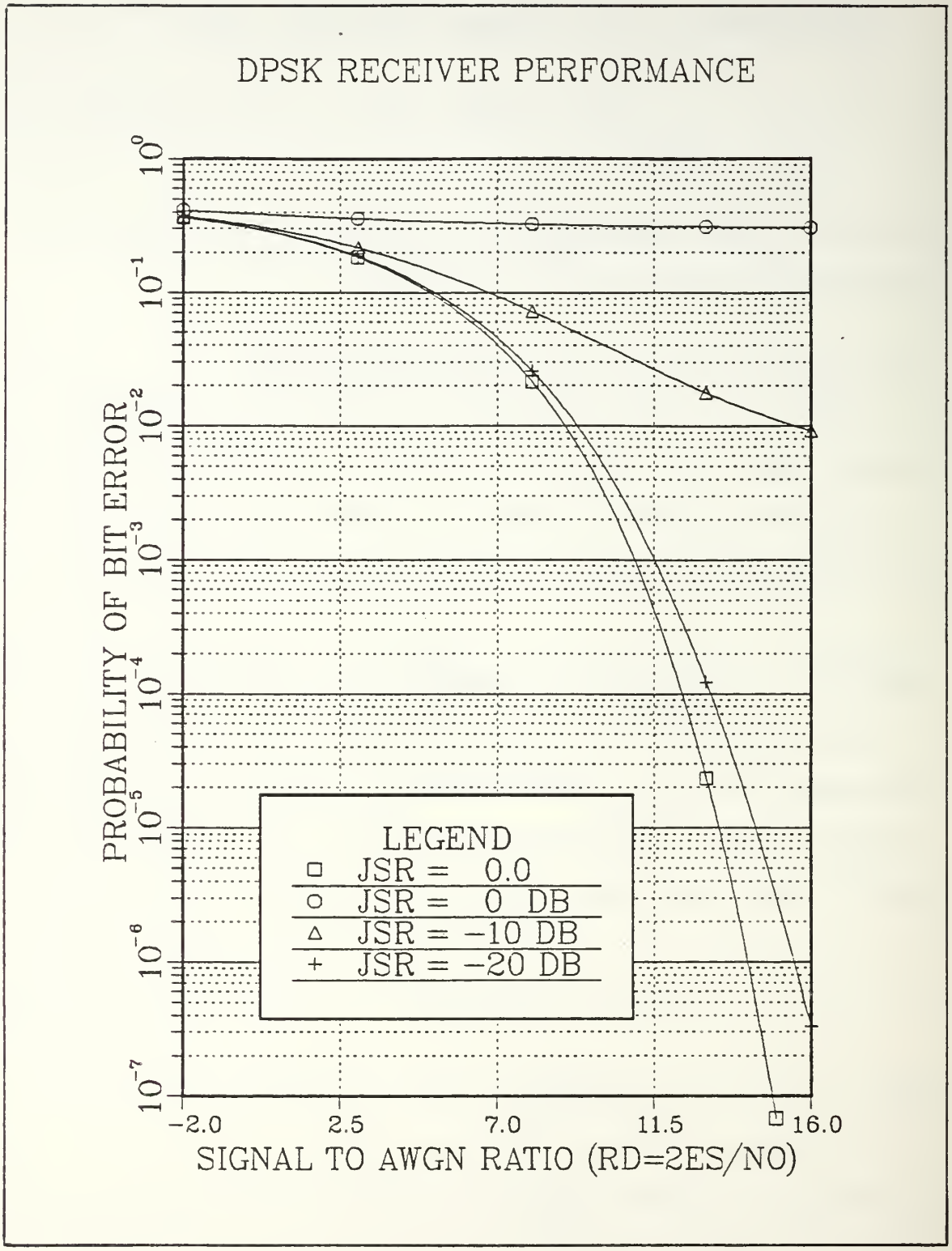

Figure 4.3 DPSK Receiver Performance

V. M-ARY QUADRATURE AMPLITUDE MODULATION

The types of spectrally efficient signaling techniques discussed in this thesis provide bandwidth efficiency proportional to $k = \log_2 M$, where k is the number of information bits per symbol and M is the number of signaling waveforms. It is well known that for MPSK signaling over an AWGN channel, for every doubling of signal phases beyond eight phases, approximately a 6 dB increase in average transmitted signal power is required in order to maintain the same error rate performance. Quadrature Amplitude Modulation (QAM) is a signaling technique that can reduce this penalty by using a combination of signal amplitudes and phases in order to transmit the M symbols consisting of k bits each.

A. 16 QAM RECEIVER PERFORMANCE

The waveforms of the 16 QAM signaling scheme can be represented by

$$x_c(t) = A_1 m_1(t)\cos[2\pi f_0 t+\alpha] + A_2 m_2(t)\sin[2\pi f_0 t+\alpha] \qquad (5.1)$$

where $A_1 = A_2 = a$ and a is an amplitude parameter, α is the transmitter phase uncertainty which is modeled as fixed but arbitrary and $m_1(t)$ and $m_2(t)$ are the digital data signals of duration T_s seconds having amplitudes

$$m_1(t) = \pm 1, \pm 3$$

$$0 \leq t \leq T_s \tag{5.2}$$

$$m_2(t) = \pm 1, \pm 3$$

If we now define

$$\phi_1(t) \triangleq \sqrt{2/T_s} \cos[2\pi f_0 t + \alpha] \tag{5.3}$$

$$\phi_2(t) \triangleq \sqrt{2/T_s} \sin[2\pi f_0 t + \alpha] \tag{5.4}$$

and

$$A \triangleq a\sqrt{T_s/2} \tag{5.5}$$

then the signals of the 16 QAM signal set can be expressed as

$$s_i(t) = Am_1(t)\phi_1(t) + Am_2(t)\phi_2(t) \quad i = 1,2,\ldots,16 \tag{5.6}$$

where the four values that $m_1(t)$ and $m_2(t)$ can individually take, generate 16 unique signals that can be represented as vectors on a two-dimensional plane as shown in Figure (5.1).

The average energy of the signal set is

$$\bar{E}_s = 10\ A^2 \tag{5.7}$$

so that the parameter A in terms of $\bar{E}_s$ becomes

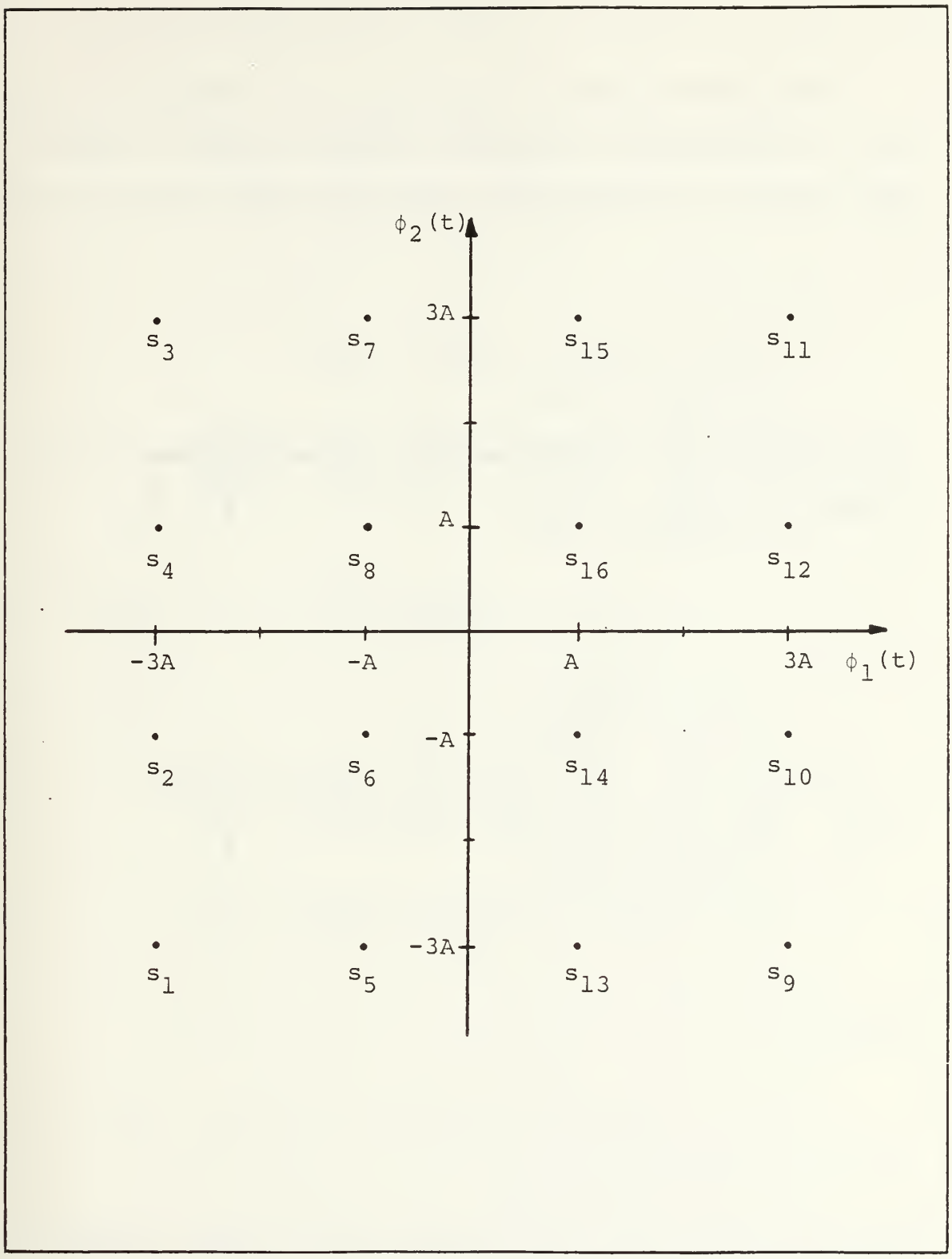

Figure 5.1 Signal Space Diagram for 16 QAM Signaling

$$A = \sqrt{\bar{E}_s/10} \tag{5.8}$$

The optimum receiver in minimum error probability sense for a 16 QAM scheme operating in AWGN is shown in Figure 5.2. When jamming is present, the received signal for this scheme is

$$r(t) = s_i(t) + n_w(t) + n_c(t) \tag{5.9}$$

The statistics of random variables Y_1 and Y_2 under these conditions can be shown to be

$$E\{Y_1\} = S_{i1} \tag{5.10}$$

$$E\{Y_2\} = S_{i2} \tag{5.11}$$

$$\sigma^2_{Y_1} = \sigma^2_{Y_2} = \frac{N_0}{2} + \sigma_c^2 \triangleq \sigma^2 \tag{5.12}$$

$$E\{[Y_1-E\{Y_1\}][Y_2-E\{Y_2\}]\} = 0 \tag{5.13}$$

where

$$S_{ij} = Am_j(t) \quad j = 1,2 \; ; \quad i = 1,2,\ldots,16 \tag{5.14}$$

Again, we find that Y_1 and Y_2 are statistically independent, conditionally Gaussian random variables. Therefore the joint conditional p.d.f. of Y_1 and Y_2 is

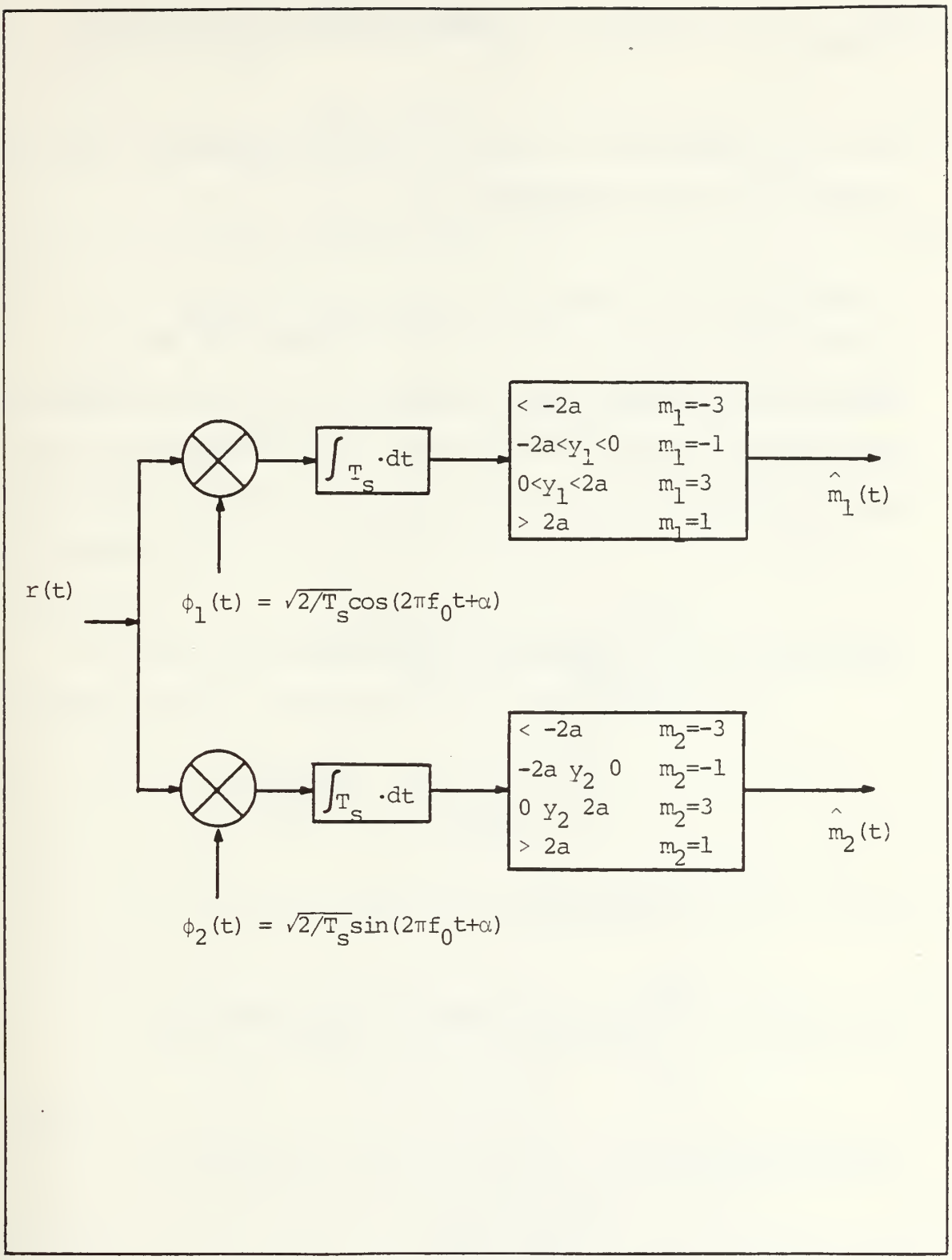

Figure 5.2 Optimum 16 QAM Receiver Structure

$$f_{Y_1Y_2|s_i(t)}(Y_1,Y_2|s_i(t)) = \frac{1}{2\pi\sigma^2}\exp\left\{-\frac{(Y_1-E\{Y_1\})^2-(Y_2-E\{Y_2\})^2}{2\sigma^2}\right\} \quad (5.15)$$

and the probability of making a correct decision, given that signal $s_i(t)$ was transmitted is

$$Pr\{c|s_i(t)\} = Pr\{L_{1\ell} < Y_1 \leq L_{1u}, L_{2\ell} < Y_2 \leq L_{2u}\} \quad (5.16)$$

where the upper and lower limits L_{ju}, $L_{j\ell}$, $j = 1,2$ must be determined for each of the signals in the signal set. In general

$$Pr\{c|s_i(t)\} = \int_{L_{1\ell}}^{L_{1u}} \frac{1}{\sqrt{2\pi\sigma^2}}\exp\{-\frac{(Y_1-S_{i1})^2}{2\sigma^2}\}dY_1$$

$$\times \int_{L_{2\ell}}^{L_{2u}} \frac{1}{\sqrt{2\pi\sigma^2}}\exp\{-\frac{(Y_2-S_{i2})^2}{2\sigma^2}\}dY_2 \quad (5.17)$$

which can be simplified to the form

$$Pr\{c|s_i(t)\} = \int_{g_1}^{g_2} \frac{1}{\sqrt{2\pi}}\exp\{-Z^2/2\}dZ \int_{h_1}^{h_2} \frac{1}{\sqrt{2\pi}}\exp\{-W^2/2\}dW \quad (5.18)$$

where the limits of integration are defined as

$$g_1 = \frac{L_{l\ell} - S_{i1}}{\sigma} \quad (5.19)$$

$$g_2 = \frac{L_{1u} - S_{i1}}{\sigma} \tag{5.20}$$

$$h_1 = \frac{L_{2\ell} - S_{i2}}{\sigma} \tag{5.21}$$

$$h_2 = \frac{L_{2u} - S_{i2}}{\sigma} \tag{5.22}$$

In order to evaluate $Pr\{c|s_i(t)\}$, we must first define the decision regions for each of the signals in the signal space. Fortunately, all of the signals in the 16 QAM signal space have decision regions which can be described by one of the subsets of the two-dimensional plane as described in Figure 5.3.

It can be shown that the conditional probabilities of correct decision associated with these regions are

$$Pr\{c|I\} = [erf_*(\gamma)]^2 \tag{5.23}$$

$$Pr\{c|II\} = [1 - 2\ erfc_*(\gamma)]^2 \tag{5.24}$$

$$Pr\{c|III\} = erf_*(\gamma)[1 - 2\ erfc_*(\gamma)] \tag{5.25}$$

where

$$\gamma \triangleq \frac{A}{\sigma} = \sqrt{R_D/10(1+R_DR_J)} \tag{5.26}$$

and

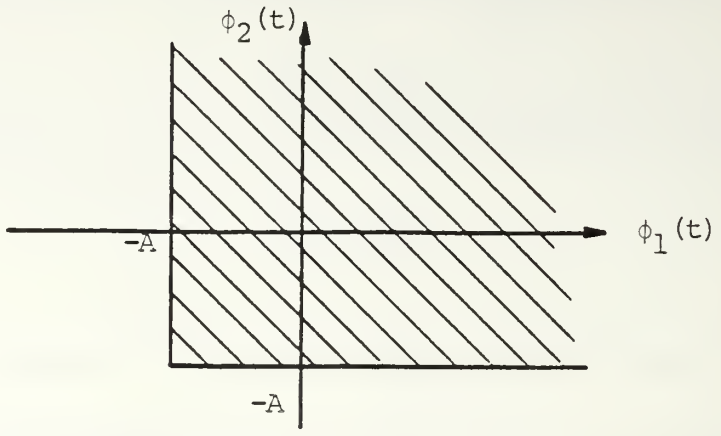

(a) Translated Type I Decision Region

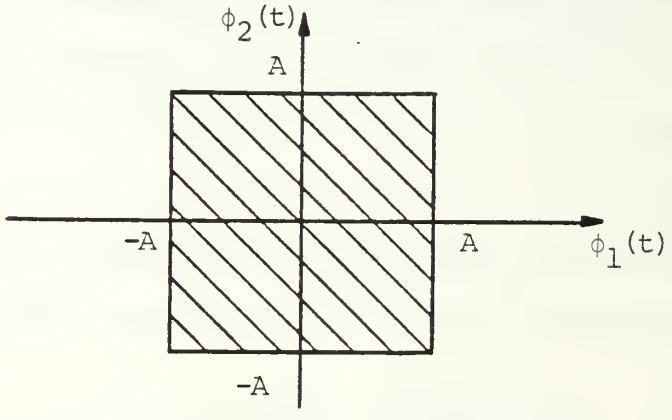

(b) Translated Type II Decision Region

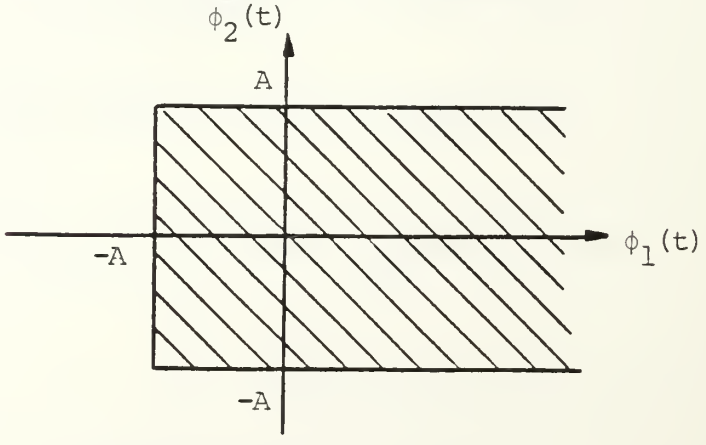

(c) Translated Type III Decision Region

Figure 5.3 16 QAM Decision Regions

$$R_D = 2\bar{E}_s/N_0 \quad \text{(Signal to Noise Ratio)} \tag{5.27}$$

$$R_J = \sigma_c^2/\bar{E}_s \quad \text{(Jamming to Signal Ratio)} \tag{5.28}$$

Assuming all signals are equally likely to be transmitted, we have

$$\Pr\{\varepsilon\} = 1 - \{\tfrac{1}{4}\,\mathrm{erf}_*^2(\gamma) + [\tfrac{1}{2} - \mathrm{erfc}_*(\gamma)]^2 + \mathrm{erf}_*(\gamma)\,[\tfrac{1}{2} - \mathrm{erfc}_*(\gamma)]\} \tag{5.29}$$

Observe that if no jamming is present, equation (5.29) becomes

$$\Pr\{\varepsilon\} = 1 - \{\tfrac{1}{4}\,\mathrm{erf}_*^2(\sqrt{E_s/5N_0}) + [\tfrac{1}{2} - \mathrm{erfc}_*(\sqrt{E_s/5N_0})]^2$$

$$+ \mathrm{erf}_*(\sqrt{E_s/5N_0})\,[\tfrac{1}{2} - \mathrm{erfc}_*(\sqrt{E_s/5N_0})]\} \tag{5.30}$$

which is the probability of error for a 16 QAM signaling scheme in AWGN. Furthermore, if the jamming power becomes infinitely large,

$$\lim_{R_J \to \infty} \Pr\{\varepsilon\} = \frac{15}{16} \tag{5.31}$$

which is expected for a signaling set with 16 equiprobable signals.

We now wish to maximize the jammer's effect on the 16 QAM signaling technique. Taking derivatives of equation (5.29) with respect to γ yields

$$\frac{d}{d\gamma} \Pr\{\varepsilon\} = -\frac{3}{2\sqrt{2\pi}} \exp\{-\gamma^2/2\}[3\mathrm{erf}_*(\gamma) - 1] \tag{5.32}$$

Since γ is always positive and $\mathrm{erf}_*(\gamma)$ takes on values ranging from 0.5 to 1.0 for γ between 0 and ∞, respectively.

$$\frac{d}{d\gamma} \Pr\{\varepsilon\} < 0 \quad \text{for all } \gamma \tag{5.33}$$

Therefore, in order to maximize $\Pr\{\varepsilon\}$, γ must be made as small as possible, which further implies making R_J or equivalently σ_c^2 as large as possible for fixed $\bar{E}_s$. Recalling that

$$\sigma_c^2 = \int_{-\infty}^{\infty} S_c(f) |\Phi_1'(f)|^2 df \tag{5.34}$$

we again have for a power-constrained jammer

$$S_c(f) = P_c |\Phi_1'(f)|^2 \tag{5.35}$$

so that

$$\sigma_c^2 = \frac{1}{16} P_c \tag{5.36}$$

Figure 5.4 shows the performance for the 16 QAM receiver as a function of SNR for fixed values of JSR.

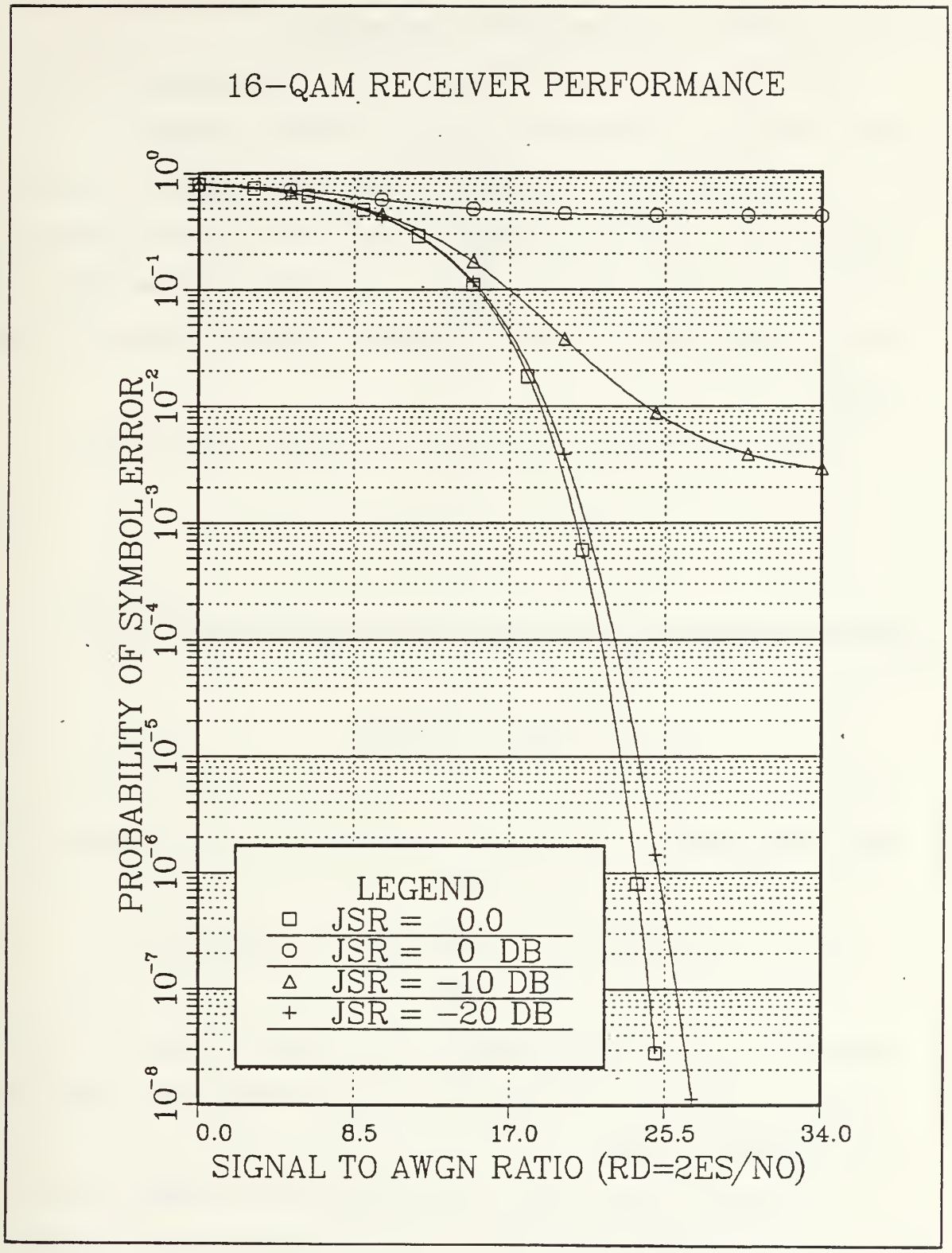

Figure 5.4 16 QAM Receiver Performance

B. 64 AND 256 QAM RECEIVER PERFORMANCE

The concepts just developed for 16 QAM signaling can most easily be extended to 64 and 256 QAM systems.

The signal space diagram for 64 QAM signaling is shown in Figure 5.5. The signal space diagram for 64 QAM signaling contains the same Type I, Type II and Type III decision regions as in 16 QAM except that a different number of each of these exist.

Also, the average energy of the signal set is now

$$\bar{E}_s = 42\ A^2 \tag{5.37}$$

and as a result, γ of equation (5.26) is given by

$$\gamma = \frac{A}{\sigma} = \sqrt{R_D/42(1+R_D R_J)} \tag{5.38}$$

The total probability of a correct decision now becomes

$$Pr\{c\} = \frac{1}{64}[4Pr\{c|I\} + 36Pr\{c|II\} + 24Pr\{c|III\}] \tag{5.39}$$

where $Pr\{c|I\}$, $Pr\{c|II\}$ and $Pr\{c|III\}$ are defined by equations (5.23), (5.24) and (5.25) respectively with γ defined by equation (5.38).

The symbol error rate performance for 64 QAM is now

$$Pr\{\varepsilon\} = 1 - \frac{1}{4}\{\frac{1}{4}\,erf_*^2(\gamma)+9[\frac{1}{2}-erfc_*(\gamma)]^2+3erf_*(\gamma)[\frac{1}{2}-erfc_*(\gamma)]\} \tag{5.40}$$

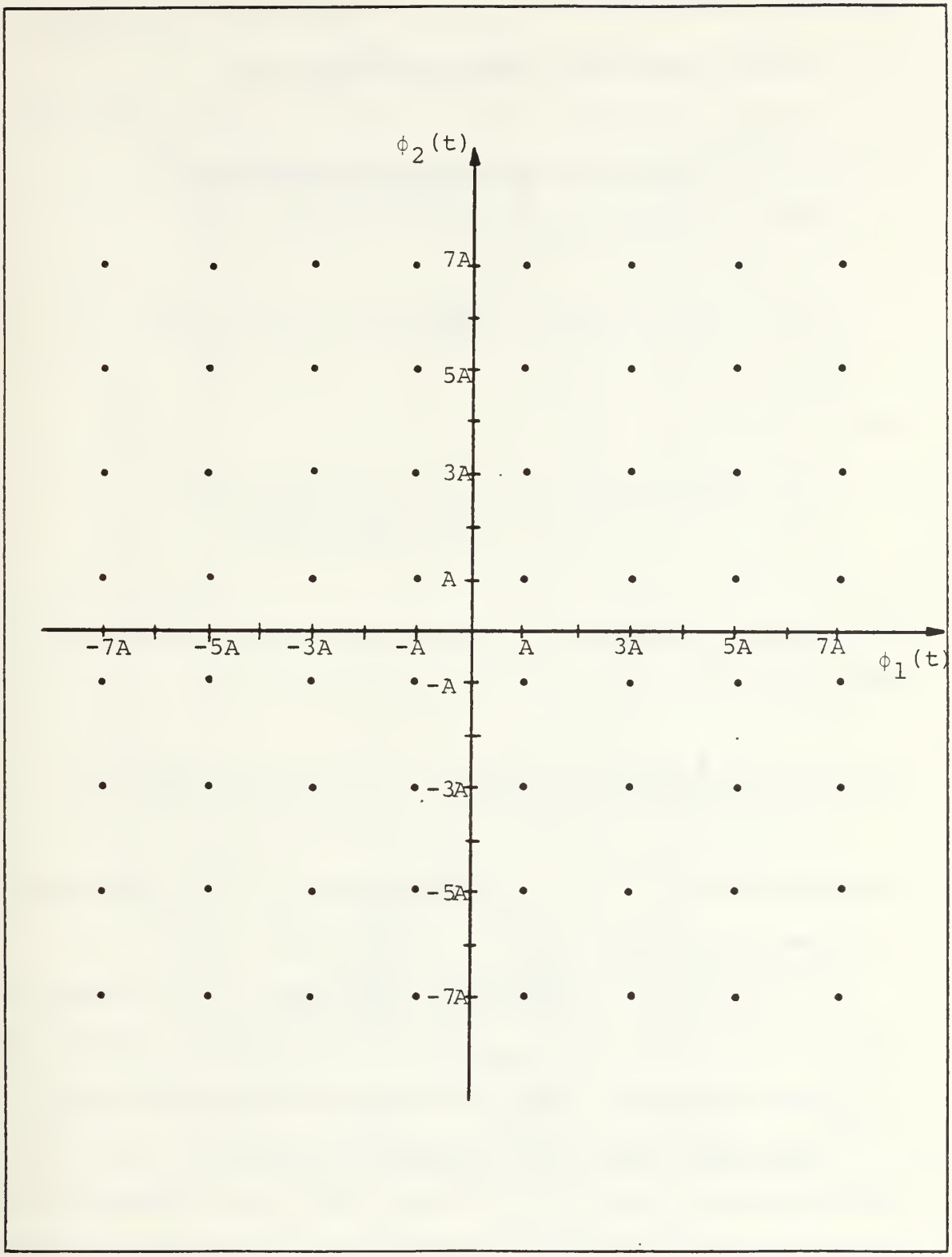

Figure 5.5 Signal Space Diagram for 64 QAM Signaling

Receiver performance curves for 64 QAM signaling described by equation (5.40) are shown in Figure 5.6.

The same technique can be used to find the error performance of 256 QAM in colored noise jamming.

The average signal set energy is now

$$\bar{E}_s = \frac{1359}{8} A^2 \tag{5.41}$$

and

$$\gamma = \frac{A}{\sigma} = \sqrt{8R_D/1359(1+R_D R_J)} \tag{5.42}$$

so that the symbol error probability for 256 QAM signaling becomes

$$Pr\{\varepsilon\} = 1 - \frac{7}{16}\left\{\frac{1}{28}\,erf_*^2(\gamma)+7\left[\frac{1}{2}-erfc_*(\gamma)\right]^2+erf_*(\gamma)\left[\frac{1}{2}-erfc_*(\gamma)\right]\right\} \tag{5.43}$$

The corresponding receiver performance for 256 QAM signaling is shown in Figure 5.7.

It can easily be shown that the symbol error probabilities for both 64 and 256 QAM systems yield expected results under limiting conditions. That is, if no jamming is present, classical AWGN performance results are obtained and if the jamming power grows without bound, the error probability tends toward the maximum value for a set of M equiprobable signals, namely (M-1)/M.

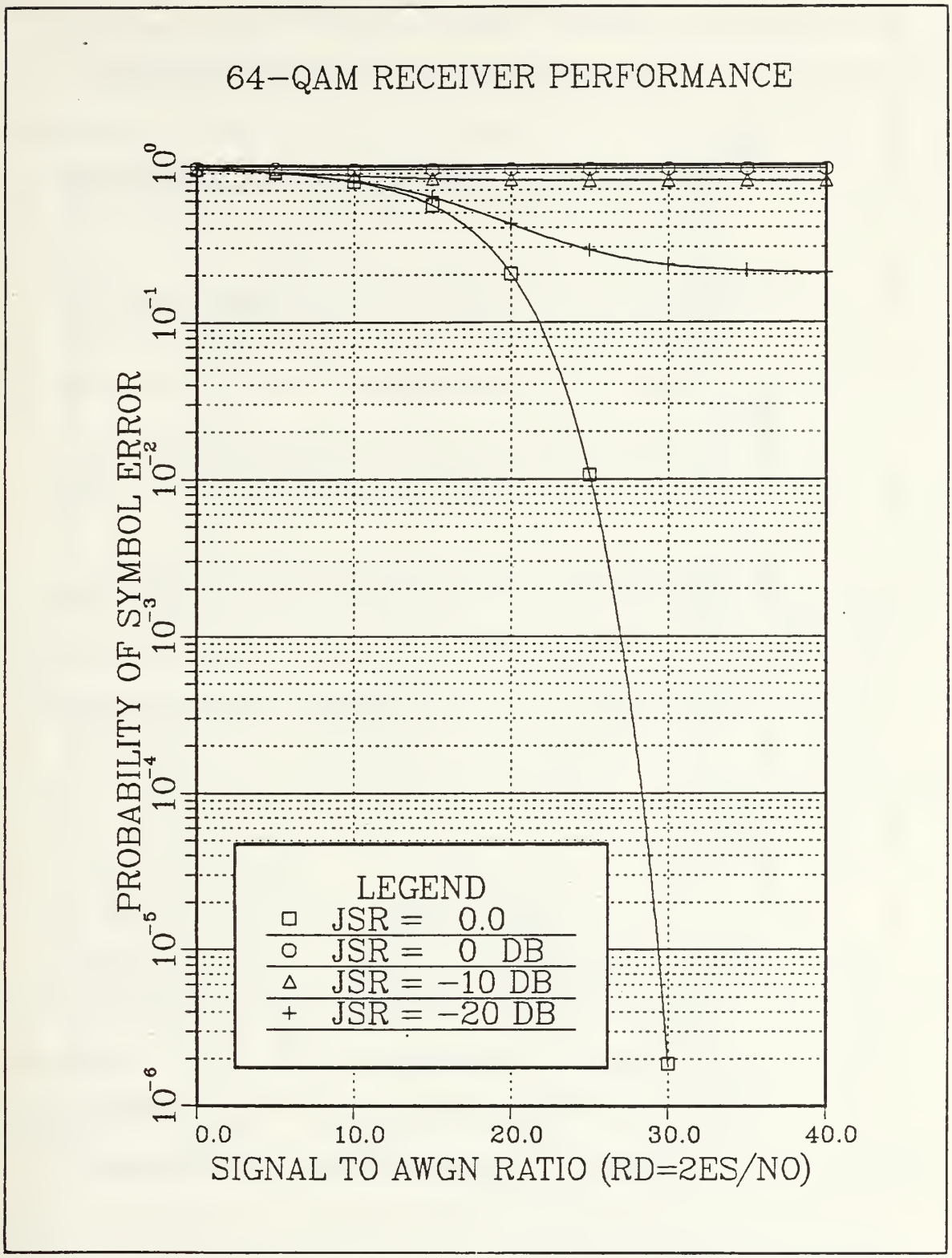

Figure 5.6 64 QAM Receiver Performance

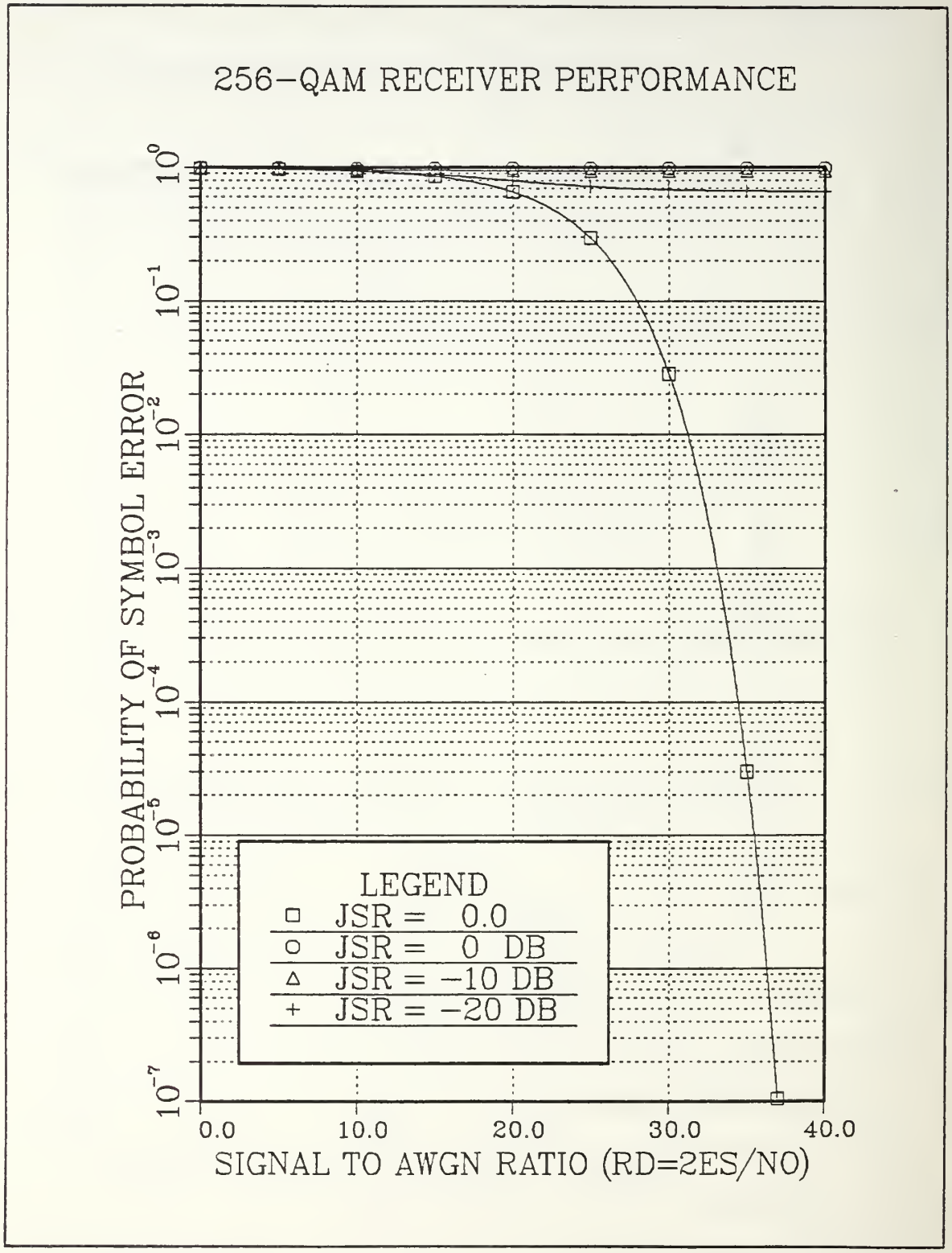

Figure 5.7 256 QAM Receiver Performance

For the 64 and 256 QAM systems, jammer optimization requires finding the derivative of the symbol error probability expressions, equations (5.40) and (5.43) with respect to R_J or equivalently γ. For the 64 QAM system the derivative yields

$$\frac{d}{d\gamma} Pr\{\varepsilon\} = \frac{-7}{8\sqrt{2\pi}} \exp\{-\gamma^2/2\}[7erf_*(\gamma)-3] < 0 \quad \text{for all } \gamma \tag{5.44}$$

and similarly for the 256 QAM system the result is

$$\frac{d}{d\gamma} Pr\{\varepsilon\} = \frac{-15}{32\sqrt{2\pi}} \exp\{-\gamma^2/2\}[15erf_*(\gamma)-7] < 0 \quad \text{for all } \gamma \tag{5.45}$$

so that the mathematical expression for the optimized colored noise jamming spectrum is the same for both 64 and 256 QAM signaling as that developed for the 16 QAM system, namely

$$S_c(f) = P_c|\Phi_1'(f)|^2 \tag{5.46}$$

C. 32 QAM RECEIVER PERFORMANCE

Unlike the 16, 64 and 256 QAM cases, 32 QAM signaling does not have all the same decision region types previously considered. This can be observed by examining the signal space diagram for 32 QAM signaling shown in Figure 5.8.

As can be seen, the perpendicular bisectors which define the optimum decision regions have changed slightly due to the lack of "corner" signals. However, there still exist only three distinct types of decision regions, two of which

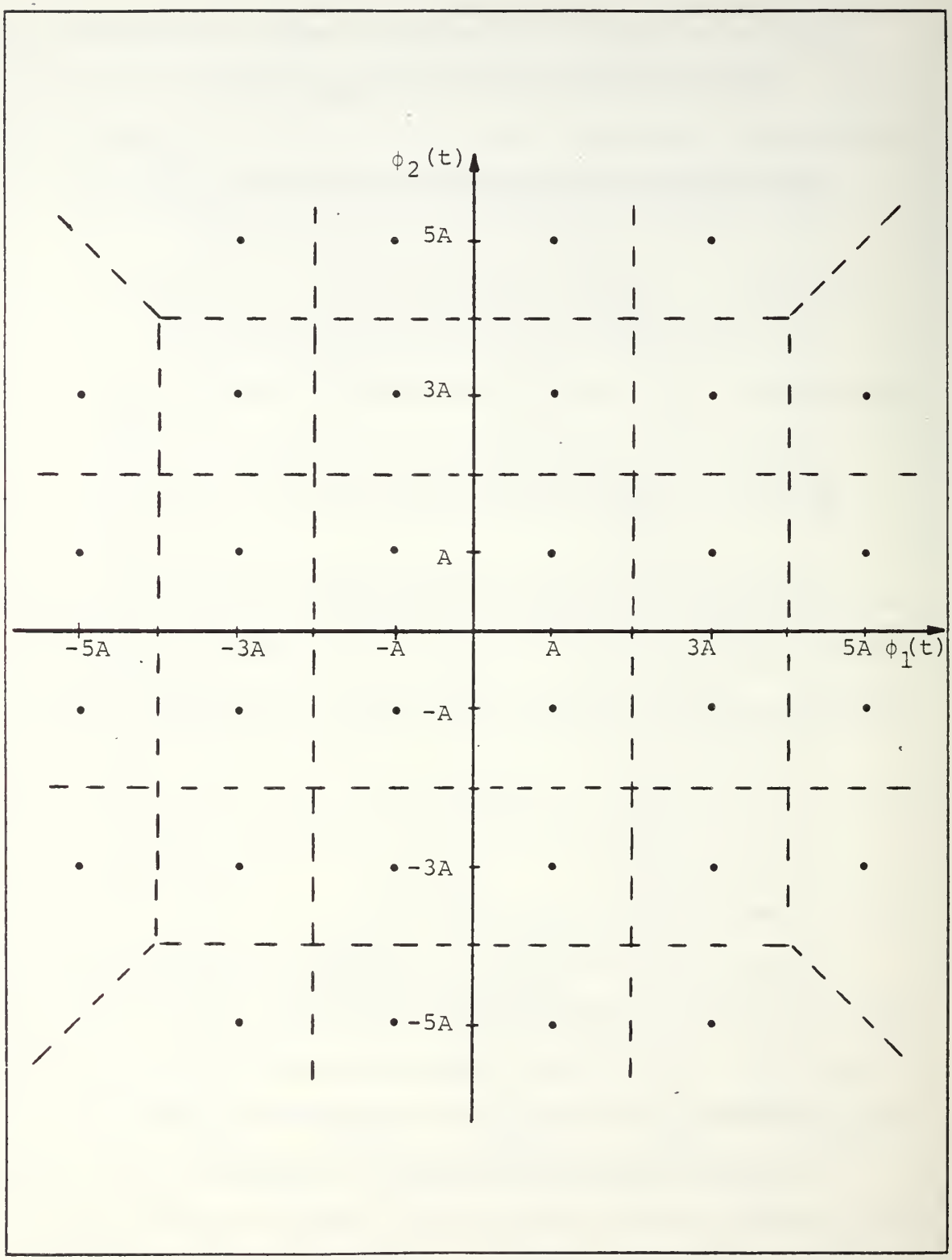

Figure 5.8 Signal Space Diagram for 32 QAM Signaling

are identical to those considered previously. The Type II and Type III decision regions shown in Figure 5.3 are consistent for 16, 32, 64 and 256 QAM cases. A new Type I decision region must be considered for the 32 QAM signaling case. Figure 5.9 shows this new Type I decision region.

From the geometry of this Type I decision region, the probability of making a correct decision given that the transmitted signal lies in a Type I decision region in the absence of noise is

$$\Pr\{c|I\} = \Pr\{-A \leq N_1, -A \leq N_2 \leq (N_1+2A)\} \tag{5.47}$$

which results in

$$\Pr\{c|I\} = \text{erf}_*^2\left(\frac{A}{\sigma}\right) - \int_{-A/\sigma}^{\infty} \frac{1}{\sqrt{2\pi}} \exp\{-x^2/2\}\text{erfc}_*\left(x+\frac{2A}{\sigma}\right)dx \tag{5.48}$$

The average energy of the signal set is

$$\bar{E}_s = 20\ A^2 \tag{5.49}$$

so that now

$$\gamma = \frac{A}{\sigma} = \sqrt{R_D/20(1+R_D R_J)} \tag{5.50}$$

The total probability of a correct decision is now

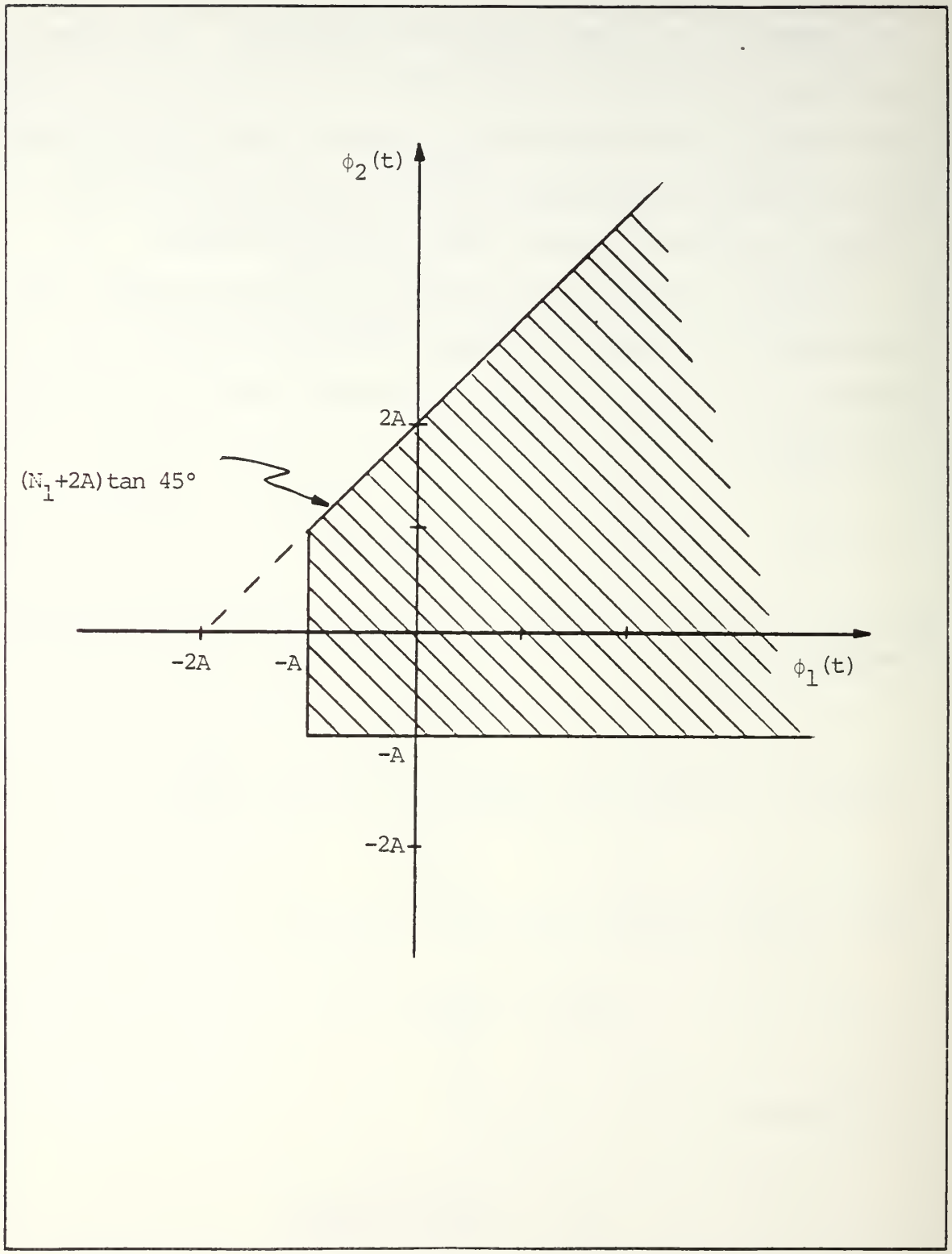

Figure 5.9 Translated Type I Decision Region for 32 QAM

$$\Pr\{c\} = \frac{1}{32}[8\Pr\{c|I\} + 16\Pr\{c|II\} + 8\Pr\{c|III\}] \tag{5.51}$$

where $\Pr\{c|II\}$ and $\Pr\{c|III\}$ are defined by equations (5.24) and (5.25) respectively with γ given by equation (5.50). The probability of a symbol error is

$$\Pr\{\varepsilon\} = 1 - \frac{1}{4}[2+11\mathrm{erf}_*^2(\gamma)-9\mathrm{erf}_*(\gamma) - \int_{-\gamma}^{\infty} \frac{1}{\sqrt{2\pi}} \exp\{-x^2/2\}\mathrm{erfc}_*(x+2\gamma)dx] \tag{5.52}$$

Performance curves for a 32 QAM receiver structure operating in colored noise jamming are shown in Figure 5.10.

The optimized jammer is found by first taking the derivative of equation (5.52) with respect to γ. This derivative shows

$$\frac{d}{d\gamma}\Pr\{\varepsilon\} = \frac{-1}{4\sqrt{2\pi}}\left\{[23\mathrm{erf}_*(\gamma)-10]\exp\{-\gamma^2/2\}+\exp\{-\gamma^2\}\right\} < 0 \tag{5.53}$$

for all γ

and therefore we again have for a power constrained jammer

$$S_c(f) = P_c|\Phi_1'(f)|^2 \tag{5.54}$$

so that

$$\sigma_c^2 = \frac{1}{16} P_c \tag{5.55}$$

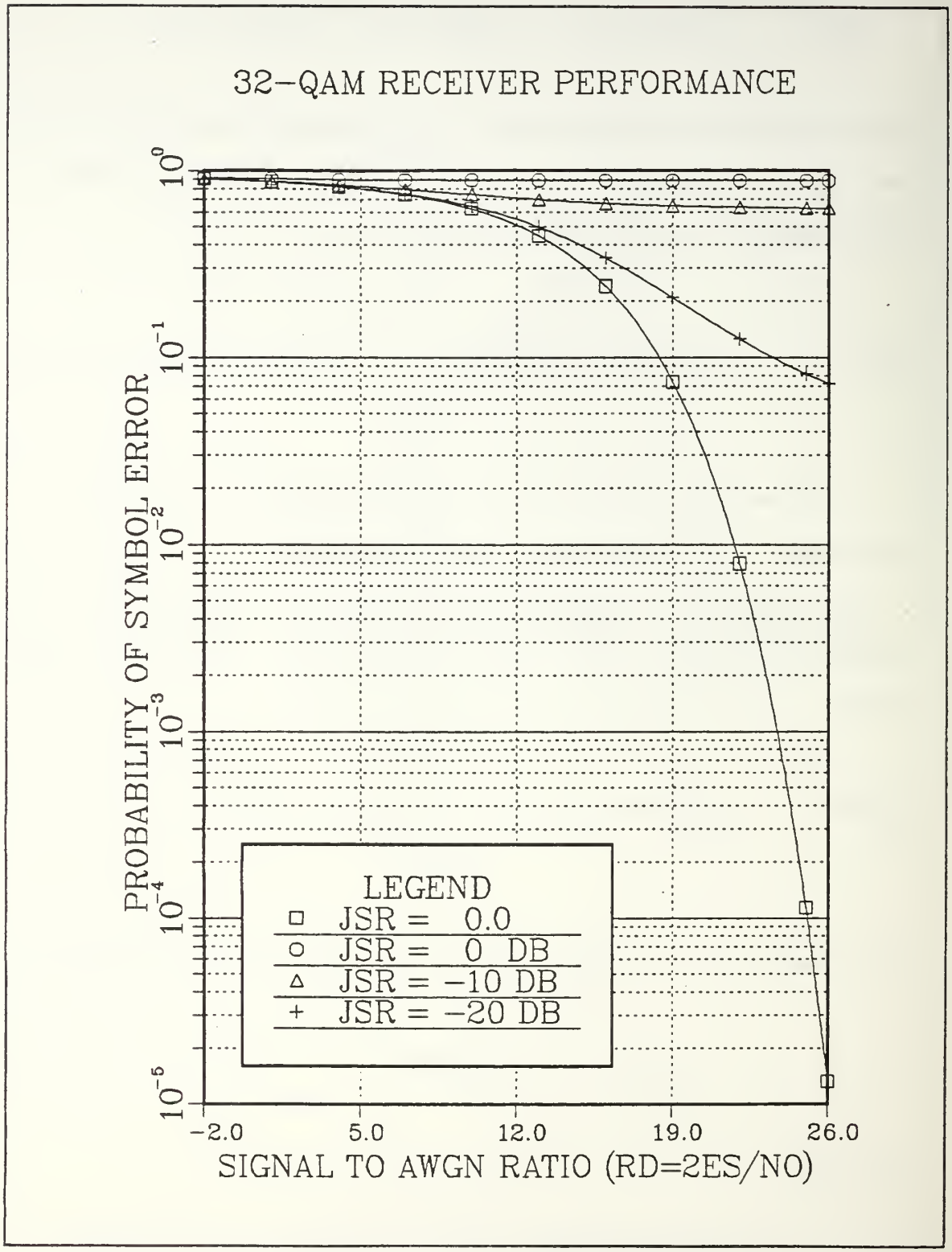

Figure 5.10 32 QAM Receiver Performance

VI. A SPECIAL CASE OF QUADRATURE AMPLITUDE MODULATION: 16-STATE AM/PM SIGNALING

The 16-state AM/PM signaling scheme is a CCITT recommended technique used in 9600 bit/sec. voice band modems [Ref. 7]. This technique can be considered to be a modification of the 16 QAM signaling previously considered. Because of its potential application in digital radio transmission, its performance in the presence of AWGN and colored noise jamming is analyzed.

A. RECEIVER PERFORMANCE IN COLORED NOISE JAMMING

The signal space diagram for 16-state AM/PM signaling is shown in Figure 6.1.

The waveforms of this signaling technique can be expressed in terms of the quadrature components, namely

$$x_c(t) = A_1 m_1(t)\cos[2\pi f_0 t+\alpha] + A_2 m_2(t)\sin[2\pi f_0 t+\alpha] \qquad (6.1)$$

where $A_1 = A_2 = a$, α is the transmit phase uncertainty and $m_1(t)$ and $m_2(t)$ are the digital data signals of duration T_s seconds with amplitudes

$$m_1(t) = \pm 1, \pm 3, \pm 5$$

$$0 \leq t \leq T_s \qquad (6.2)$$

$$m_2(t) = \pm 1, \pm 3, \pm 5$$

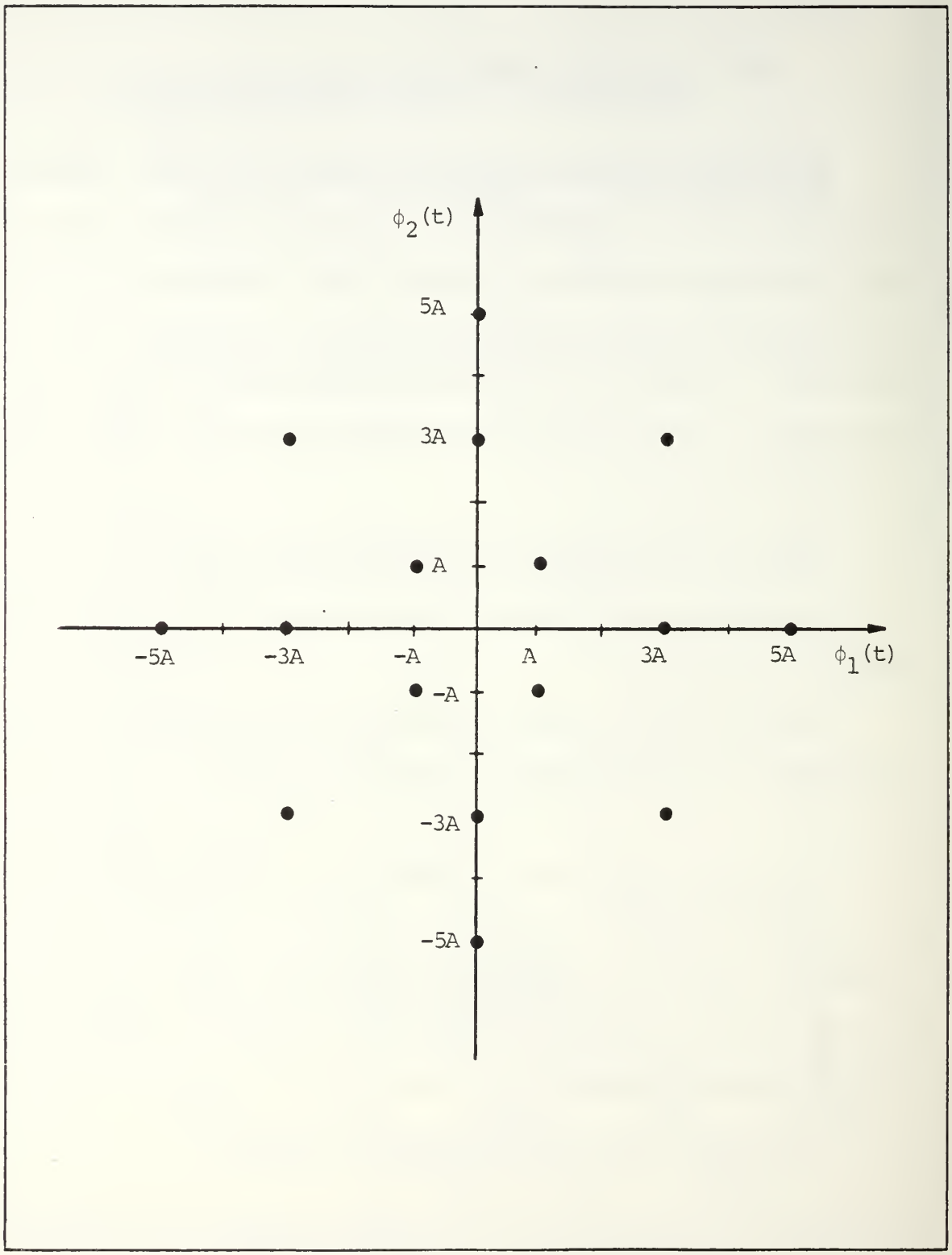

Figure 6.1 Signal Space Diagram for 16-State AM/PM Signaling

The 16 signals can be expressed as

$$s_i(t) = Am_1(t)\phi_1(t) + Am_2(t)\phi_2(t) \quad i = 1,2,\ldots,16 \qquad (6.3)$$

where $\phi_1(t)$, $\phi_2(t)$ and A are defined by equations (5.3), (5.4) and (5.5) respectively.

The average energy of the signal set is

$$\bar{E}_s = \frac{27}{2} A^2 \quad \rightarrow \quad A = \sqrt{2\bar{E}_s/27} \qquad (6.4)$$

The optimum decision regions defined by the perpendicular bisectors of the signals in the signal space diagram produce four unique segments of the two-dimensional space as Figure 6.2 shows.

As can be seen from Figure 6.2, the optimum decision regions are unusually shaped. The receiver logic necessary to determine whether a received signal is within its corresponding decision region would be extremely complex. Since such an optimum receiver would be either impractical or uneconomical to implement, we consider instead suboptimum decision regions associated with this scheme as shown in Figure 6.3. Such decision regions could be implemented in logic very easily by first determining the received signal component along $\phi_1(t)$ and $\phi_2(t)$.

This is demonstrated by the receiver structure shown in Figure 6.4, where amplitude and phase information of the received signal is extracted.

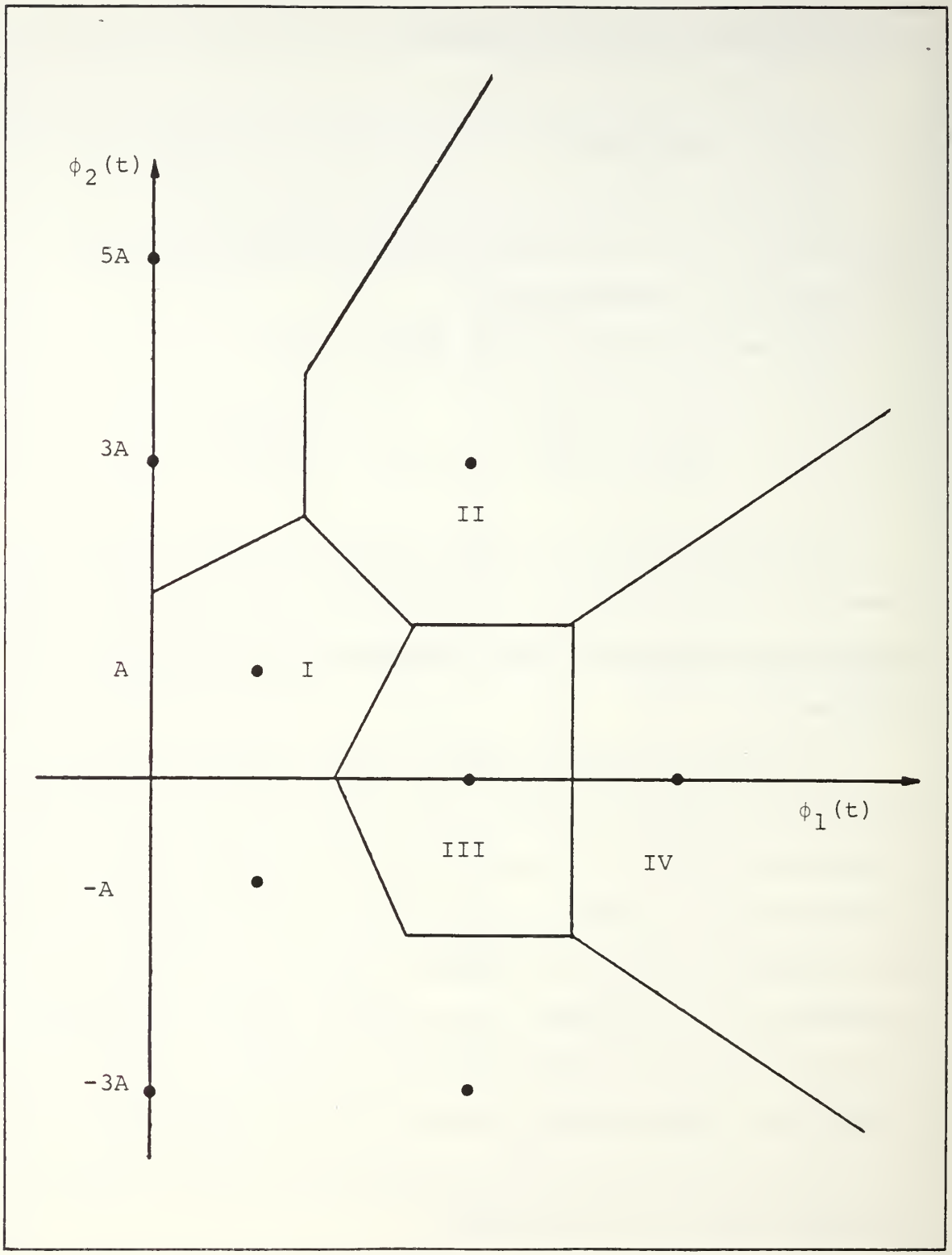

Figure 6.2 Optimum Decision Regions for 16-State AM/PM Signaling

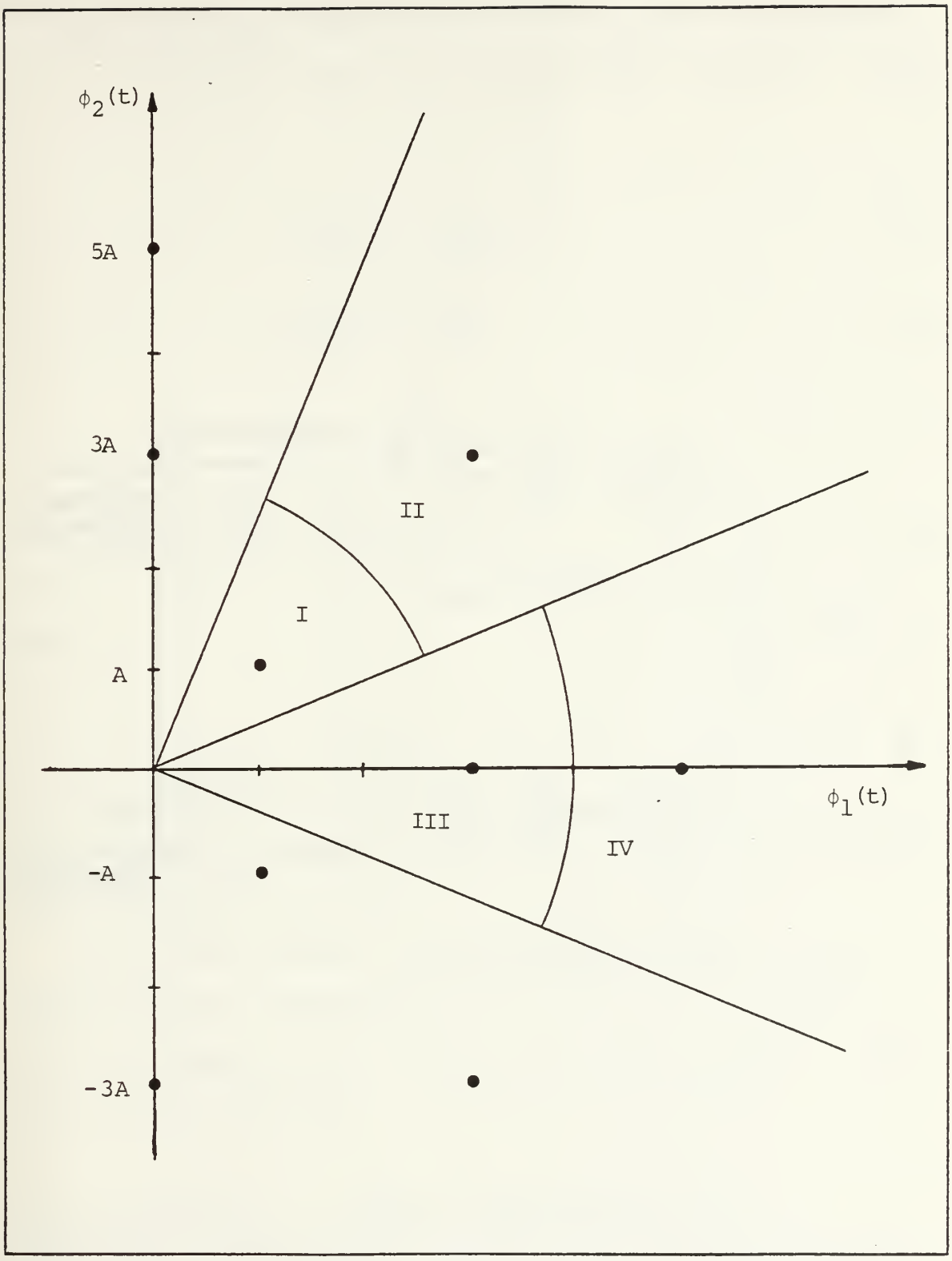

Figure 6.3 Suboptimum Decision Regions for 16-State AM/PM Signaling

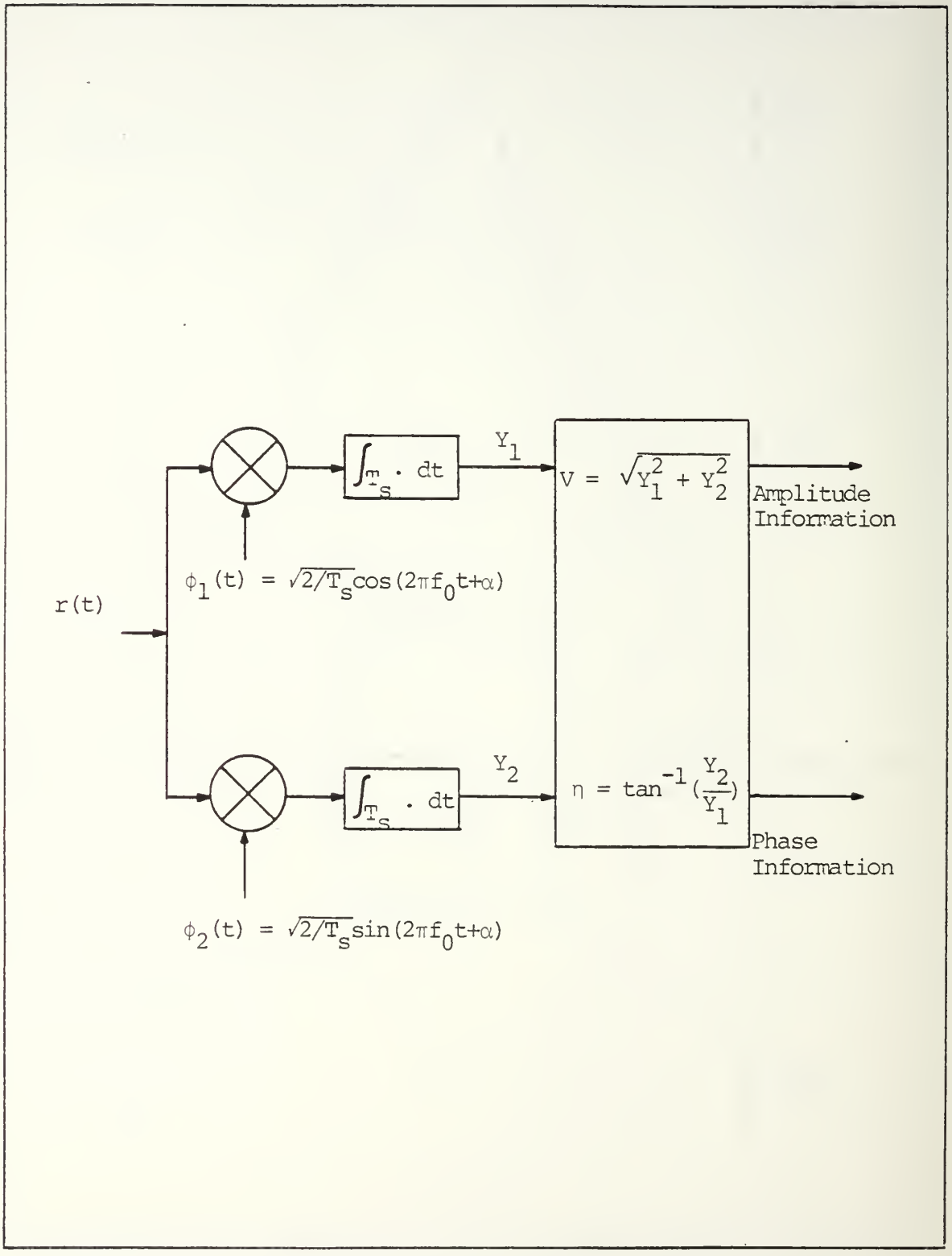

Figure 6.4 Receiver Structure for Suboptimum 16-State AM/PM Signaling

The statistical description of the random variables Y_1 and Y_2 is similar to that developed for QAM signaling. That is,

$$E\{Y_1\} = S_{i1} \tag{6.5}$$

$$E\{Y_2\} = S_{i2} \tag{6.6}$$

$$\sigma_{Y_1}^2 = \sigma_{Y_2}^2 = \frac{N_0}{2} + \sigma_c^2 \triangleq \sigma^2 \tag{6.7}$$

$$E\{[Y_1-E\{Y_1\}][Y_2-E\{Y_2\}]\} = 0 \tag{6.8}$$

where

$$S_{ij} = Am_j(t) \quad j = 1,2 \quad i = 1,2,\ldots,16 \tag{6.9}$$

Again, Y_1 and Y_2 are statistically independent conditionally Gaussian random variables.

Just as was carried out for MPSK signaling, a double random variable transformation is used so as to generate random variables V and η having conditional probability density function given by

$$f_{V,H|s_i(t)}(v,\eta|s_i(t)) = \frac{v}{2\pi\sigma^2}\exp\{-\frac{1}{2\sigma^2}[v-\sqrt{E_i}\cos(\eta-\beta_i)]^2\}$$

$$\times \exp\{-\frac{1}{2\sigma^2}[E_i\sin^2(\eta-\beta_i)]\} \tag{6.10}$$

$$v \geq 0, \quad 0 \leq \eta \leq 2\pi$$

where

$$V = \sqrt{Y_1^2 + Y_2^2} \; ; \quad \eta = \tan^{-1}(Y_2/Y_1) \tag{6.11}$$

and

$$E_i = \sqrt{S_{i1}^2 + S_{i2}^2} \tag{6.12}$$

$$\beta_i = \tan^{-1}(S_{i2}/S_{i1}) \tag{6.13}$$

We now compute the probability of a correct decision associated with each of the four types of decision regions described in Figure 6.3.

For the Type I decision region

$$\Pr\{c|I\} = \Pr\{0 \leq V \leq 2A\sqrt{2}, \frac{\pi}{8} \leq \eta \leq \frac{3\pi}{8}\} \tag{6.14}$$

which with the use of the conditional p.d.f. of equation (6.10) results in

$$\Pr\{c|I\} = \frac{1}{8}\exp\{-d^2\} - \frac{1}{\pi}\exp\{-5d^2\} \int_0^{\pi/8} \exp\{4d^2 \cos\psi\}d\psi$$

$$+ \frac{2}{\sqrt{\pi}}\, d \int_0^{\pi/8} \cos\psi \exp\{-d^2\sin^2\psi\}\left[\mathrm{erf}_*(\sqrt{2}d\cos\psi) - \mathrm{erfc}_*(\sqrt{2}d\{2-\cos\psi\})\right]d\psi \tag{6.15}$$

where

$$d \triangleq \frac{A}{\sigma} = \sqrt{2R_D/27(1+R_D R_J)} \tag{6.16}$$

For the Type II decision region

$$\Pr\{c|II\} = \Pr\{2A\sqrt{2} \leq V \leq \infty, \frac{\pi}{8} \leq \eta \leq \frac{3\pi}{8}\} \tag{6.17}$$

which yields

$$\Pr\{c|II\} = \frac{1}{\pi}\exp\{-13d^2\}\int_0^{\pi/8} \exp\{12d^2\cos\psi\}d\psi$$

$$+ \frac{6}{\sqrt{\pi}}\, d \int_0^{\pi/8} \cos\psi \exp\{-9d^2\sin^2\psi\}\,\mathrm{erfc}_*\{\sqrt{2}d(2-3\cos\psi)\}d\psi \tag{6.18}$$

where again equation (6.10) has been used to obtain equation (6.18). Equation (6.10) is also used to evaluate

$$\Pr\{c|III\} = \Pr\{0 \leq V \leq 4A, -\frac{\pi}{8} \leq \eta \leq \frac{\pi}{8}\} \tag{6.19}$$

for the Type III decision region, thus yielding

$$\Pr\{c|III\} = \frac{1}{8}\exp\{-\frac{9}{2}d^2\} - \frac{1}{\pi}\exp\{-\frac{25}{2}d^2\}\int_0^{\pi/8} \exp\{12d^2\cos\eta\}d\eta$$

$$+ \frac{6}{\sqrt{2\pi}}\, d\int_0^{\pi/8} \cos\eta \exp\{-\frac{9}{2}d^2\sin^2\eta\}[\mathrm{erf}_*(3d\cos\eta) - \mathrm{erfc}_*(d\{4-3\cos\eta\})]d\eta \tag{6.20}$$

and finally, for the Type IV decision region

$$\Pr\{c|IV\} = \Pr\{4A \leq V \leq \infty, -\frac{\pi}{8} \leq \eta \leq \frac{\pi}{8}\} \tag{6.21}$$

for which

$$\Pr\{c|IV\} = \frac{1}{\pi}\exp\{-\frac{41}{2}d^2\}\int_0^{\pi/8}\exp\{20d^2\cos\eta\}d\eta$$

$$+\frac{10}{\sqrt{2\pi}}d\int_0^{\pi/8}\cos\eta\exp\{-\frac{25}{2}d^2\sin^2\eta\}\operatorname{erfc}_*(d\{4-5\cos\eta\})d\eta \tag{6.22}$$

Assuming equal prior probability of transmission for all signals, the total probability of a correct decision is obtained by evaluating

$$\Pr\{c\} = \frac{1}{16}[4\Pr\{c|I\} + 4\Pr\{c|II\} + 4\Pr\{c|III\} + 4\Pr\{c|IV\}] \tag{6.23}$$

which after some simplification becomes

$$\Pr\{c\} = \frac{1}{32}\exp\{-d^2\} + \frac{1}{32}\exp\{-\frac{9}{2}d^2\} - \frac{1}{4\pi}\exp\{-d^2\}\int_0^{\pi/8}\exp\{-8d^2\sin^2\frac{\psi}{2}\}d\psi$$

$$- \frac{1}{4\pi}\exp\{-\frac{1}{2}d^2\}\int_0^{\pi/8}\exp\{-24d^2\sin^2\frac{\eta}{2}\}d\eta + \frac{1}{4\pi}\exp\{-d^2\}\int_0^{\pi/8}\exp\{-24d^2\sin^2\frac{\psi}{2}\}d\psi$$

$$+ \frac{1}{4\pi}\exp\{-\frac{1}{2}d^2\}\int_0^{\pi/8}\exp\{-40d^2\sin^2\frac{\eta}{2}\}d\eta$$

$$+ \frac{d}{2\sqrt{\pi}}\int_0^{\pi/8}\cos\psi\exp\{-d^2\sin^2\psi\}[\mathrm{erf}_*(\sqrt{2}\cos\psi) - \mathrm{erfc}_*(\sqrt{2}d[2-\cos\psi])]d\psi$$

$$+ \frac{6d}{4\sqrt{2\pi}}\int_0^{\pi/8}\cos\eta\exp\{-\frac{9}{2}d^2\sin^2\eta\}[\mathrm{erf}_*(3d\cos\eta) - \mathrm{erfc}_*(d[4-3\cos\eta])]d\eta$$

$$+ \frac{10d}{4\sqrt{2\pi}}\int_0^{\pi/8}\cos\eta\exp\{-\frac{25}{2}d^2\sin^2\eta\}\mathrm{erfc}_*(d[4-5\cos\eta])d\eta$$

$$+ \frac{6d}{4\sqrt{\pi}}\int_0^{\pi/8}\cos\psi\exp\{-9d^2\sin^2\psi\}\mathrm{erfc}_*(\sqrt{2}d[2-3\cos\psi])d\psi \qquad (6.24)$$

This rather lengthy expression can be analyzed for the case in which the jamming power increases without bound. From equation (6.16) under these conditions d tends toward zero and

$$\lim_{d\to 0}\Pr\{c\} = \frac{1}{16} \qquad (6.25)$$

which is the expected result for a signal set with 16 equi-probable signals.

Performance curves for the suboptimum 16-state AM/PM receiver are shown in Figure 6.5.

Since the expression for the probability of a correct decision given by equation (6.24) is so mathematically involved, no attempt has been made to optimize the colored noise jammer against the 16-state AM/PM receiver. However, based on the results of Figure 6.5, it seems reasonable to assume that the optimum jamming spectrum should match the transmitted signal spectrum, just as encountered in the previous signaling schemes analyzed.

For a performance comparison of the 16-state AM/PM scheme, Figure 6.6 shows receiver performance curves for 16-QAM, 16-state AM/PM and 16-PSK signaling in an AWGN environment.

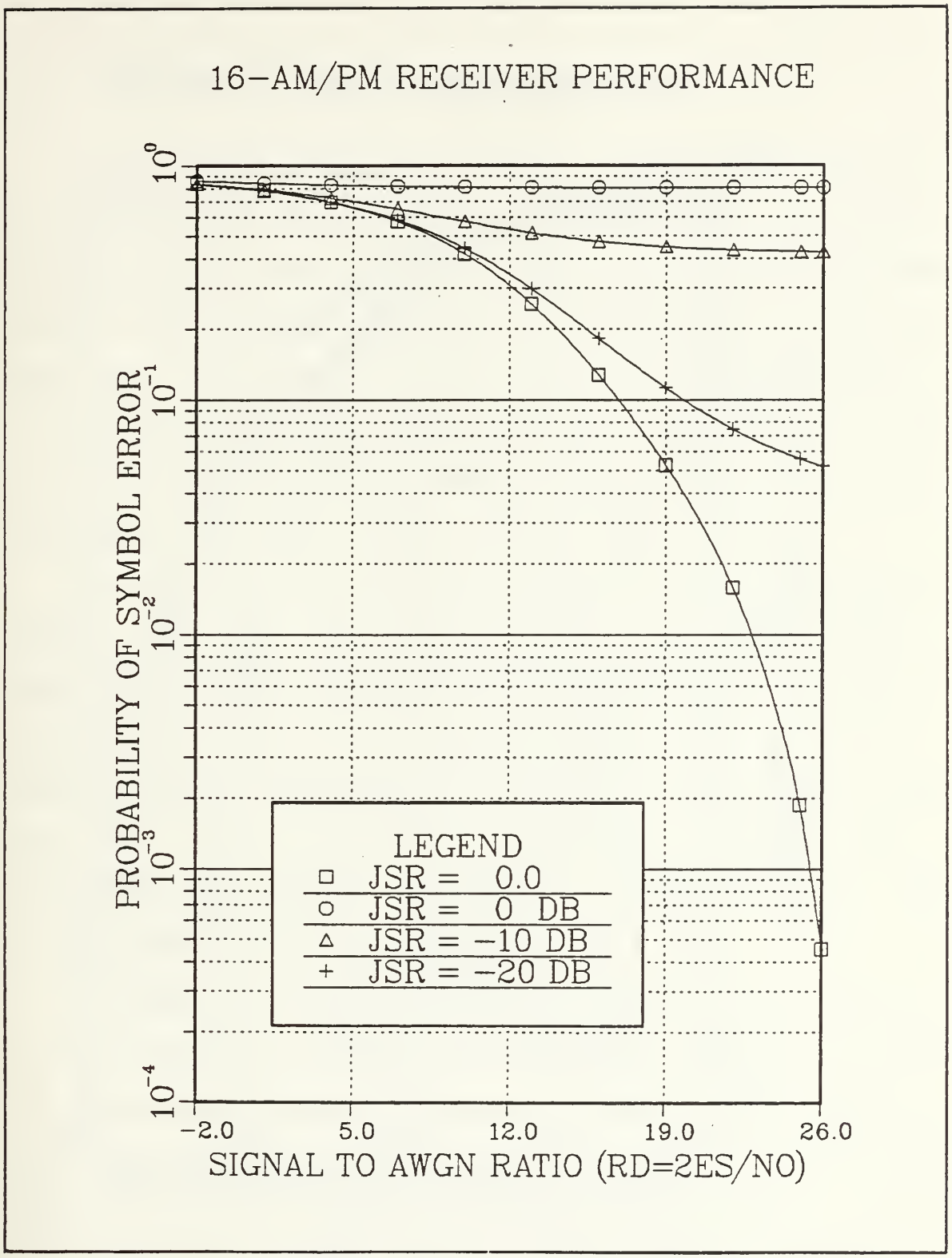

Figure 6.5 16-State AM/PM Receiver Performance

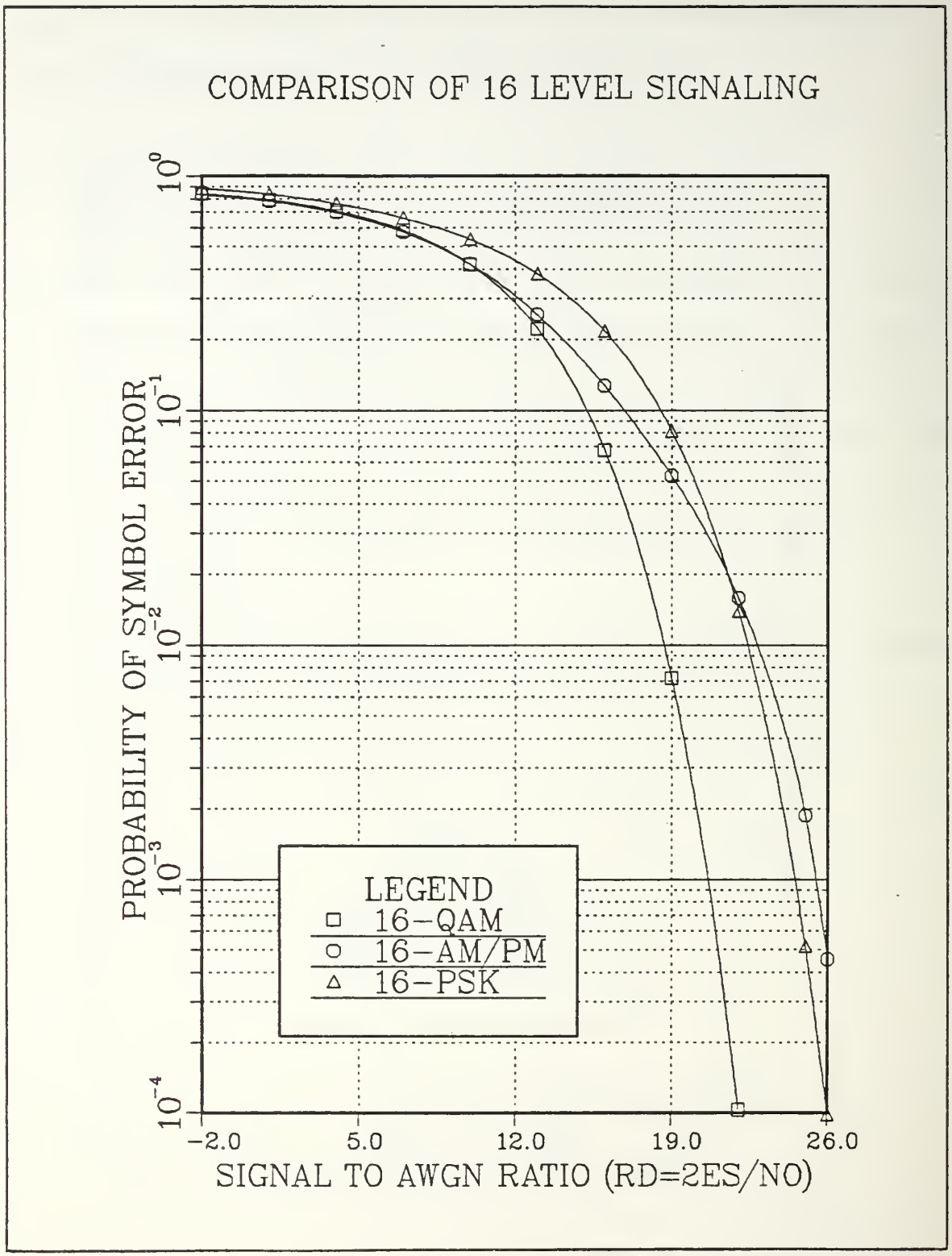

Figure 6.6 Performance Comparison of 16 Level Signaling

VII. CONCLUSIONS

In this thesis the performance of receivers assumed to be operating in the presence of both AWGN and colored noise jamming has been analyzed for several digital modulation techniques. In all except the 16-state AM/PM case, the receivers considered are optimum for discriminating amongst M signals received in an AWGN environment in the sense of minimum probability of error. Receiver symbol error probability was used throughout as the measure of receiver performance.

In addition to receiver performance analysis, optimized jamming techniques were also developed. The colored noise jammer was modeled as power limited, uncorrelated with the white channel noise and Gaussianly distributed with power spectral density determined as part of the optimization procedure. The intent of the optimization was to maximize the receiver symbol error probability while making efficient use of the jammer's available power.

In Chapter II, the MPSK receiver structure was analyzed in the presence of colored noise jamming. Figures 2.2 through 2.5 corresponding to the M = 4, 8, 16 and 32 cases respectively, all conclusively show significant receiver performance degradation in the presence of relatively low levels of colored noise jamming. Typically only a -10 dB jamming-to-signal ratio was required to increase the symbol error probability a

minimum of one order of magnitude for SNR values in the range of 15 dB to 30 dB. The M = 4 and M = 8 cases showed superior performance in the presence of jamming when compared to the M = 16 and M = 32 cases. This is not surprising since the optimum decision regions defined by the perpendicular bisectors of adjacent signals in the signal space, mathematically described by the angle θ, where $-\frac{\pi}{M} < \theta < \frac{\pi}{M}$, become smaller as M increases. The smaller the decision regions become, the more likely it is that the additive interference will produce an observation vector at the receiver which lies outside of the correct decision region thereby causing a decision error. For the MPSK modulation method, the optimum power constrained colored noise jammer was found to have a power spectral density which mimicked the power spectrum of the MPSK signal.

The general results developed in Chapter II were then applied to three special cases of MPSK signaling in Chapter III. QPSK, OQPSK and MSK are all special cases of 4-ary PSK modulation with OQPSK and MSK providing improved performance in bandlimited applications over QPSK modulation. Although the purpose and implementation differed for each, all three were found to perform identically in the jamming environment. This was not too surprising since these three signaling schemes also perform identically in AWGN-only interference. The mathematical expression for the optimum colored noise jamming waveform was also the same for these three modulation techniques. However, since the basis functions used in the

series representation of the MSK signals are different from those used in QPSK and OQPSK signaling, the actual optimum jamming spectrums differed accordingly. The optimized jamming spectrum still mimicked the signaling spectrum except that now, the signal spectrum of MSK modulation is different from that of QPSK and OQPSK modulation.

Chapter IV presented the analysis and performance evaluation of a receiver for DPSK modulation operating in the presence of AWGN and colored noise jamming. As was the case for MPSK, Figure 4.3 shows the same severe performance degradation experienced by the DPSK receiver in the presence of relatively low levels of jamming. Figure 4.3 shows the corresponding performance curves and demonstrates the degrading effect of jamming. The optimum jamming spectrum for use against DPSK modulation, as in the preceding analyses, was shown to be matched to the transmit signal spectrum.

The M-ary QAM techniques discussed in Chapter V, although showing the same general performance degradation tendency observed in the other signaling schemes, provided the best overall performance in the presence of jamming for a given value of M and JSR level of all the signaling techniques analyzed. Relating again the size of the optimum receiver decision regions to the receiver performance, QAM signals have the largest decision regions for fixed signal energy and value of M, with a smaller decrease in size of the decision region for increasing values of M, when compared to other

digital modulation schemes. Therefore, for a given SNR and symbol error probability, more signaling levels and therefore more information bits per symbol ($k = \log_2 M$) can be transmitted using M-ary QAM than using MPSK modulation, whether or not jamming is present. This improved receiver performance combined with a receiver structure implementation that is as simple as that for MPSK signaling, explains the popularity of QAM techniques in modern digital communication applications. Figures 5.4, 5.6, 5.7 and 5.10 graphically display the QAM receiver performance for M = 16, 64, 256 and 32. As before, the jamming spectrum that optimizes the colored noise jammer in QAM transmission cases is identical to that of the transmit signal spectrum.

The 16-state AM/PM signaling scheme analyzed in Chapter VI yielded several interesting results. First, the receiver structure necessary to make optimum decisions proved too complicated to practically implement. A suboptimum receiver structure was therefore selected by modifying the MPSK receiver structure in such a way that both amplitude and phase information about the observation signal vector are computed. The performance analysis was then carried out assuming that both AWGN and colored noise jamming were present in the channel. The mathematical expression for symbol error probability proved so involved that jammer optimization was not attempted. However, receiver performance graphs for the 16-state AM/PM technique using the suboptimum system described above were

generated as shown in Figure 6.5. A comparison of Figure 6.5 with Figures 2.4 and 5.4 which show 16-PSK and 16 QAM receiver performance, respectively, demonstrates that the suboptimum 16-state AM/PM receiver structure yields a performance which lies between that of 16-PSK and 16 QAM. A performance comparison of these three 16-level signaling techniques in AWGN is shown in Figure 6.6. The 16-state AM/PM suboptimum scheme performs almost as well as the QAM system at SNR levels below 12 dB, approaches the performance of PSK for SNR values between 16 dB and 22 dB, and then performs worse than both QAM and PSK for SNR values beyond 22 dB. This is partly due to the use of suboptimum rather than optimum decision regions in the 16-state AM/PM receiver. As the SNR increases, the size of the optimum decision regions increases proportionally. The size of the suboptimum decision regions, however, do not increase at a similar rate causing the receiver structure to become more suboptimum at higher SNR levels. Although no jammer optimization was performed, based on previous results, the optimum colored noise jammer spectrum would be expected to mimic the 16-state AM/PM signal spectrum. Consequently, receiver performance was determined and evaluated on the assumption that the jammer spectrum was matched to the signal spectrum.

Table 7.1 presents selected receiver performance results for each of the receiver structures analyzed. The SNR was selected corresponding to a symbol error probability of 10^{-4} in AWGN. Table 7.2 identifies the SNR penalty associated with

TABLE 7.1

COMPARATIVE RECEIVER SYMBOL ERROR PROBABILITIES

Number of Signaling Levels M	Signaling Method	SNR	JSR = 0.0	JSR = -20 dB	JSR = -10 dB
2	DPSK	12 dB	1.8×10^{-4}	5.35×10^{-4}	2.33×10^{-2}
4	QPSK	14 dB	3.93×10^{-4}	1.52×10^{-3}	5.37×10^{-2}
8	8-PSK	20 dB	1.28×10^{-4}	6.77×10^{-3}	2.48×10^{-1}
16	16-PSK	25 dB	5.17×10^{-4}	8.88×10^{-2}	5.44×10^{-1}
	16-QAM	22 dB	1.03×10^{-4}	3.25×10^{-4}	1.98×10^{-2}
	16-state AM/PM	26 dB	4.54×10^{-4}	5.21×10^{-2}	4.27×10^{-1}
32	32-PSK	31 dB	4.84×10^{-4}	3.44×10^{-1}	7.57×10^{-1}
	32-QAM	25 dB	1.14×10^{-4}	8.15×10^{-2}	6.29×10^{-1}
64	64-QAM	28 dB	1.86×10^{-4}	2.48×10^{-1}	7.97×10^{-1}
256	256-QAM	34 dB	2.26×10^{-4}	6.68×10^{-1}	9.42×10^{-1}

TABLE 7.2

SNR PENALTY FOR MAINTAINING $PR\{\varepsilon\} = 10^{-2}$ IN JAMMING

Number of Signaling Levels, M	Signaling Method	SNR Penalty for JSR = -20 dB
2	DPSK	0.5 dB
4	QPSK	0.5 dB
8	8-PSK	2 dB
16	16-PSK	>6 dB
	16-QAM	2 dB
	16-state AM/PM	>4 dB
32	32-PSK	*
	32-QAM	>10 dB
64	64-QAM	*
256	256-QAM	*

* Asymptotically approaches a $Pr\{\varepsilon\} < 10^{-2}$

maintaining a symbol error probability of 10^{-2} in a -20 dB JSR environment. As shown in all M-ary signaling techniques analyzed, symbol error probability increases with increasing M. The modulation scheme least affected by the colored noise jamming was the QAM system.

Throughout this thesis, the optimum colored noise jammer was found to require exact knowledge of the transmit signal spectrum. Without this a priori information, a suboptimum colored noise jammer would be expected to provide similar yet less effective results since the optimum jammer caused such large performance degradation with low power levels.

In summary, although the AWGN receiver is considered a general purpose receiver that performs well in many different channel environments, the results presented here show that significant performance degradation can be expected when the same system is used in a colored noise jamming environment. By the same reasoning, the colored noise jamming model used throughout this thesis has proven to be an extremely effective, power efficient jammer for use against AWGN receivers.

APPENDIX A

DETAILED INVESTIGATION OF THE PRODUCT OF $\Phi_1(-f)$ AND $\Phi_2(f)$

Let $\phi_1(t)$ and $\phi_2(t)$ be given by equation (2.3), namely

$$\phi_1(t) = \sqrt{2/T_s}\cos(2\pi f_0 t+\alpha) \quad \text{and} \quad \phi_2(t) = \sqrt{2/T_s}\sin(2\pi f_0 t+\alpha) \tag{A.1}$$

and define

$$\phi_j'(t) \triangleq \begin{cases} \phi_j(t), & 0 \leq t \leq T_s \\ 0, & \text{otherwise} \end{cases} \qquad j = 1,2 \tag{A.2}$$

so that the $\phi_j'(t)$ are defined for all time t. Thus, $\phi_j'(t)$, $j = 1,2$, can now be expressed as

$$\phi_1'(t) = p(t)\cos(2\pi f_0 t) \tag{A.3}$$

$$\phi_2'(t) = p(t)\sin(2\pi f_0 t) \tag{A.4}$$

where

$$p(t) = \begin{cases} \sqrt{2/T_s}, & 0 \leq t \leq T_s \\ 0, & \text{otherwise} \end{cases} \tag{A.5}$$

and α has been set to zero.

The Fourier Transform of p(t), namely P(f) is given by

$$P(f) = \sqrt{2/T_s}\,\frac{\sin(\pi f T_s)}{(\pi f T_s)}\,e^{-j\pi f T_s} = \sqrt{2/T_s}\,\mathrm{sinc}(fT_s)e^{-j\pi f T_s} \tag{A.6}$$

so that

$$\Phi_1'(f) = \frac{1}{2}[P(f-f_0) + P(f+f_0)]$$

$$= \frac{1}{2}\sqrt{2/T_s}[e^{-j\pi(f-f_0)T_s}\mathrm{sinc}(f-f_0)T_s$$

$$+ e^{-j\pi(f+f_0)T_s}\,\mathrm{sinc}(f+f_0)T_s] \tag{A.7}$$

and

$$\Phi_2'(f) = \frac{1}{j2}[P(f-f_0) - P(f+f_0)]$$

$$= \frac{1}{j2}\sqrt{2/T_s}[e^{-j\pi(f-f_0)T_s}\,\mathrm{sinc}(f-f_0)T_s$$

$$- e^{-j\pi(f+f_0)T_s}\,\mathrm{sinc}(f+f_0)T_s] \tag{A.8}$$

Using equations (A.7) and (A.8) the product of $\Phi_1'(-f)$ and $\Phi_2'(f)$ becomes

$$\Phi_1'(-f)\Phi_2'(f) = \frac{T_s}{j8}[e^{j2\pi f_0 T_s}S_+S_- + S_-^2 - S_+^2 - S_+S_-e^{-j2\pi f_0 T_s}] \tag{A.9}$$

where

$$S_+ \triangleq \text{sinc}(f+f_0)T_s \quad \text{and} \quad S_- \triangleq \text{sinc}(f-f_0)T_s \tag{A.10}$$

Through factoring we can show

$$\Phi_1'(-f)\Phi_2'(f) = \frac{T_s}{j8}[S_- e^{j\pi f_0 T_s} - S_+ e^{-j\pi f_0 T_s}][S_+ e^{j\pi f_0 T_s} + S_- e^{-j\pi f_0 T_s}] \tag{A.11}$$

Expanding the terms in the brackets yields

$$G(f) \triangleq \Phi_1'(-f)\Phi_2'(f) = \frac{T_s}{8}\{j[\text{sinc}^2(f+f_0)T_s - \text{sinc}^2(f-f_0)T_s]$$

$$+ \text{sinc}[(f+f_0)T_s]\text{sinc}[(f-f_0)T_s]\sin(2\pi f_0 T_s)\} \tag{A.12}$$

and similarly

$$G(-f) \triangleq \Phi_1'(f)\Phi_2'(-f) = \frac{T_s}{8}\{-j[\text{sinc}^2(f+f_0)T_s - \text{sinc}^2(f-f_0)T_s]$$

$$+ \text{sinc}[(f-f_0)T_s]\text{sinc}[(f+f_0)T_s]\sin(2\pi f_0 T_s)\} \tag{A.13}$$

Observe that

$\text{Im}\{G(f)\}$ is an odd function

$\text{Re}\{G(f)\}$ is an even function

Therefore

$$\int_{-\infty}^{\infty} S_c(f)G(f)df = \int_{-\infty}^{\infty} S_c(f)[\mathrm{Re}\{G(f)\}+j\ \mathrm{Im}\{G(f)\}]df$$

$$= \int_{-\infty}^{\infty} S_c(f)\mathrm{Re}\{G(f)\}df \simeq 0 \qquad \text{(A.14)}$$

since

$$\mathrm{sinc}[(f-f_0)T_s]\mathrm{sinc}[(f+f_0)T_s] \simeq 0 \qquad \text{(A.15)}$$

LIST OF REFERENCES

1. Ziemer, Rodger E. and Peterson, Roger L., Digital Communications and Spread Spectrum Systems, pp. 198-213, MacMillan, 1985.

2. Lindsey, W.C. and Simon, M.K., Telecommunication System Engineering, pp. 228-231, Prentice Hall, 1973.

3. Feher Kamilo, Digital Communications, Satellite/Earth Station Engineering, pp. 162-168, Prentice Hall, 1981.

4. Pasupathy, Subbarayan, "Minimum Shift Keying: A Spectrally Efficient Modulation," IEEE Communications Magazine, July 1979.

5. Proakis, John G., Digital Communications, pp. 171-178, McGraw-Hill, 1983.

6. Arthurs, E. and Dym, H., "On the Optimum Detection of Digital Signals in the Presence of White Gaussian Noise--A Geometric Interpretation and a Study of Three Basic Data Transmission Systems," IRE Transactions on Communications Magazine, pp. 346-353, December 1962.

7. Smith, David R., Digital Transmission Systems, pp. 296-301, Van Nostrand, 1985.

INITIAL DISTRIBUTION LIST

		No. Copies
1.	Defense Technical Information Center Cameron Station Alexandria, Virginia 22304-6145	2
2.	Library, Code 0142 Naval Postgraduate School Monterey, California 93943-5002	2
3.	Department Chairman, Code 62 Department of Electrical and Computer Engineering Naval Postgraduate School Monterey, California 93943-5000	1
4.	Professor Daniel Bukofzer, Code 62Bh Department of Electrical and Computer Engineering Naval Postgraduate School Monterey, California 93943-5000	6
5.	Professor Paul Moose, Code 62Me Department of Electrical and Computer Engineering Naval Postgraduate School Monterey, California 93943-5000	1
6.	Captain Barry L. Shoop RD #1, Box 296B Ashland, Pennsylvania 17921	5

DUDLEY KNOX LIBRARY
NAVAL POSTGRADUATE SCHOOL
MONTEREY CALIFORNIA 93943-6002

220346

Thesis
S4833 Shoop
c.1 An analysis of coherent and differentially coherent digital receivers in the presence of colored noise interference.

Thesis
S4833 Shoop
c.1 An analysis of coherent and differentially coherent digital receivers in the presence of colored noise interference.

220346

thesS4833
An analysis of coherent and differential
3 2768 000 75708 2
DUDLEY KNOX LIBRARY